Cell Reports
Methods

Article

Engineering lymphatic collecting vessel phenotypes through combined hyaluronic acid cues and oscillatory shear stress

Graphical abstract

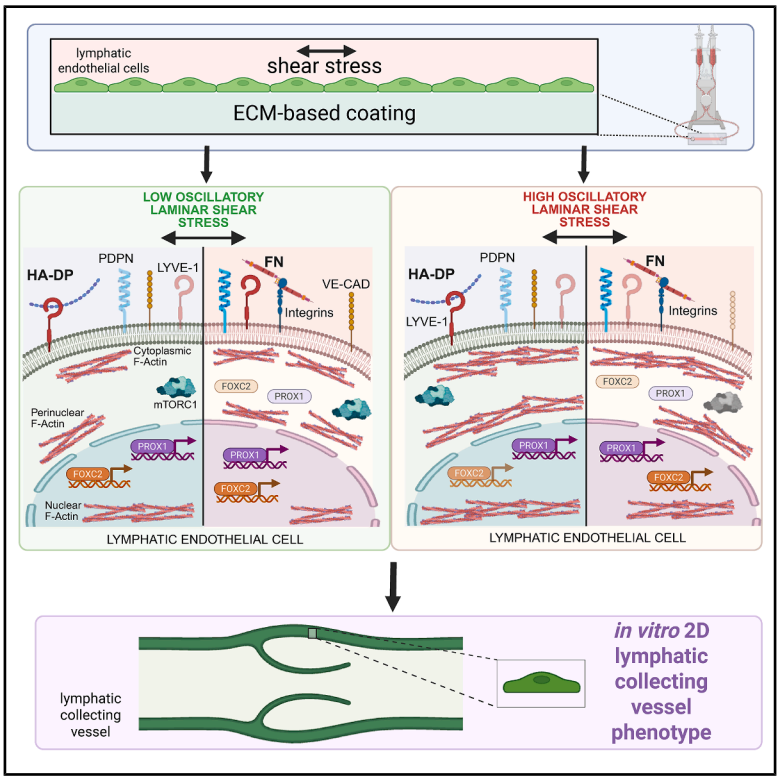

Highlights

- We present a microfluidic device-based approach for lymphatic vessel engineering
- Approach integrates hyaluronic acid coating with oscillatory flow
- Reveals ECM-dependent regulation of lymphatic mechanotransduction
- Platform supports engineering of both 2D and 3D collecting vessel models

Authors

N. Keilany Lightsey, Grace Fluskey, Brenda Cruz-Gonzalez, Fei Fan, Sanjoy Saha, Eva Hall, Donny Hanjaya-Putra

Correspondence

dputra1@nd.edu

In brief

To advance lymphatic vessel engineering, Lightsey at el. develop a microfluidic device-based approach that integrates physiologically relevant extracellular matrix cues with oscillatory shear stress. Using human lymphatic endothelial cells cultured on dopamine-modified hyaluronic acid or fibronectin, this approach reveals how the matrix-flow interactions drive mechanotransduction, collecting vessel specification, and lymphatic morphogenesis.

Lightsey et al., 2026, Cell Reports Methods 6, 101574
November 16, 2026
https://doi.org/10.1016/j.crmeth.2026.101574

CellPress

Please cite this article in press as: Lightsey et al., Engineering lymphatic collecting vessel phenotypes through combined hyaluronic acid cues and oscillatory shear stress, Cell Reports Methods (2026), https://doi.org/10.1016/j.crmeth.2026.101574

Cell Reports Methods

CellPress
OPEN ACCESS

Article

Engineering lymphatic collecting vessel phenotypes through combined hyaluronic acid cues and oscillatory shear stress

N. Keilany Lightsey,[1] Grace Fluskey,[2] Brenda Cruz-Gonzalez,[1] Fei Fan,[1] Sanjoy Saha,[1] Eva Hall,[1] and Donny Hanjaya-Putra[1,2,3,4,5,*]

[1]Bioengineering Graduate Program, University of Notre Dame, Notre Dame, IN 46556, USA
[2]Aerospace and Mechanical Engineering, University of Notre Dame, Notre Dame, IN 46556, USA
[3]Chemical and Biomolecular Engineering, University of Notre Dame, Notre Dame, IN 46556, USA
[4]Center for Stem Cell and Regenerative Medicine, University of Notre Dame, Notre Dame, IN 46556, USA
[5]Lead contact
*Correspondence: dputra1@nd.edu
https://doi.org/10.1016/j.crmeth.2026.101574

MOTIVATION Complications in the lymphatic system (i.e., lymphedema, cancer metastasis, impaired wound healing, cardiovascular disease, etc.) have become increasingly prevalent, but there are limited *in vitro* lymphatic engineering models that can provide the *in vivo* complexity of the biomechanical and biochemical signaling required for proper collecting lymphatic vessel function. To address this, we introduce an extracellular matrix-based hyaluronic acid coating along with various oscillatory laminar shear stress levels to induce an increasingly lymphatic collecting vessel phenotype for modeling and engineering purposes.

SUMMARY

The engineering of a 3D lymphatic collecting vessel has been of recent interest due to the lack of treatments for lymphatic valve disruptions. While oscillatory shear stress has been shown to regulate lymphatic collecting vessel morphogenesis, its effect in the context of physiologically relevant extracellular matrix remains elusive. In this study, we used a microfluidic device to elucidate the effect of oscillatory shear stress on human lymphatic endothelial cells cultured on dopamine-modified hyaluronic acid or fibronectin. Here, we show that hyaluronic acid can synergistically enhance mechanoresponsive morphological changes, activate cytoskeleton localization, induce nuclear expression of key mechanosensitive markers (*PROX1* and *FOXC2*), amplify mechanotransduction pathways (*VE-CAD* and *mTORC1*), and downregulate capillary lymphatic markers (*PDPN* and *LYVE-1*). These results highlight the potential of hyaluronic acid-based materials for the generation of 2D and 3D lymphatic collecting vessel models.

INTRODUCTION

The lymphatic system is an essential component of the circulatory system that helps maintain tissue fluid homeostasis as well as transport immune cells and performs other regulatory functions in the human body. Thus, there are many complications that can arise in the lymphatic system such as lymphatic drainage disruption (e.g., lymphedema), cancer metastasis, and impaired wound healing. Current treatment options for these complications are limited and do not resolve the impaired lymphatic vasculature that contributes to these pathologies.[1] In recent years, the use and development of lymphatic tissue engineering strategies have been explored to treat and model all these complications.[1–3] These strategies include the use of biomaterials, biochemical cues, co-culturing methods, various cell sources, mechanical stimuli, or a combination of any of these to induce lymphangiogenesis (i.e., the process of creating new lymphatic vessels) either *in vivo* or *in vitro*.[1–4] Many of these mentioned strategies have demonstrated promising results in engineering lymphatic capillaries[3,5–13]; however, these vessels resemble initial lymphatic vessels rather than collecting lymphatic vessels within the lymphatic system.

Collecting lymphatic vessels are the vessels within the lymphatic system that are responsible for actively transporting lymph to the lymph nodes and, eventually, blood circulation.[14–16] These vessels are segmented into lymphangions that have unidirectional, intraluminal bi-leaflet valves that prevent backflow of lymph and assist in maintaining the forward flow of lymph during lymphangion contractions caused by surrounding lymphatic smooth muscles cells and other tissues.[14,15,17–20]

Please cite this article in press as: Lightsey et al., Engineering lymphatic collecting vessel phenotypes through combined hyaluronic acid cues and oscillatory shear stress, Cell Reports Methods (2026), https://doi.org/10.1016/j.crmeth.2026.101574

Recently, it has been found that the defects in valve development and/or collecting vessel maintenance can lead to lymphedema and possibly contribute to other pathologies (obesity, fibrosis, chronic inflammation, tumor metastasis, etc.).[14,15,18] Thus, engineering a functional collecting lymphatic vessel, both *in vitro* and *in vivo*, can provide a physiologically relevant and more effective platform for treatments and disease modeling.

The use of biomaterials is of particular interest as it can mimic the extracellular matrix (ECM) properties that are necessary for collecting vessel and lymphatic valve formation. Previous studies have found that the accumulation of specific ECM proteins are found in the early stages of collecting vessel specification and lymphatic valve formation/maturation.[21,22] *In vitro,* lymphatic endothelial cells (LECs) cultured on different ECM coatings have exhibited varying growth rates and differed in their expression of identifying markers.[23,24] Fibronectin (FN), one of the most frequently used coatings for *in vitro* LEC culture, has demonstrated increased LEC adhesion and more proliferating nuclei compared with LEC cultures in uncoated environments.[24,25] Previous studies have also demonstrated that mutant variants of fibronectin serve as an essential ligand for the unique LEC receptor integrin-α9 and that this interaction is necessary for proper LEC adhesion and migration.[22,24] Another component of ECMs *in vivo*, collagen, is less commonly used as an *in vitro* ECM coating for LECs due to its ability to provide structure that can guide LEC growth.[24] The ability of biomaterials to affect lymphangiogenesis demonstrates that ECM components are promising coatings for *in vitro* culture and that incorporating ECM components is necessary to engineer an *in vivo* functional collecting lymphatic vessel. Hyaluronic acid (HA) is an essential component of the ECM, and synthetic HA has been found to preserve LEC phenotype *in vitro* by enhancing key lymphatic receptors and interact with LYVE-1 (lymphatic vessel endothelial hyaluronan receptor 1; a homolog of CD44).[24] Though not commonly explored, previous studies have found that low-molecular-weight (LMW) HA is associated with the induction of lymphangiogenesis in LECs,[26] interacts with LYVE-1 receptors to transmit signals,[27] and modulates cell spreading/migration.[28] In addition to promoting lymphangiogenesis and preserving lymphatic characteristics, HA's tunable stiffness, chemical modifiability, and non-immunogenicity also serve to make HA a promising candidate for tissue engineering.[23,24,29–32] For these reasons, exploring the use of HA as a material that can mimic the ECM in addition to other factors that promote lymphangiogenesis (i.e., mechanical stimulation, co-culturing, or biochemical cues) could advance the engineering of a collecting lymphatic vessel.

The lymphatic system is constantly exposed to shear stress in the body, and the LECs present within the vessels are sensitive and respond to these physiological shear stresses. The LECs within the lymphatic capillaries experience laminar shear stress, while the LECs within the collecting vessel more frequently experience oscillatory shear stress (OSS).[15] This oscillatory flow is often classified as a disturbed flow and can be modeled *in vitro* with a laminar flow moving in a bidirectional manner.[14,16,33] Furthermore, previous studies have found that the presence of a disturbed flow contributes to the development of lymphatic valves within collecting vessels *in vivo*, and OSS at physiological rates can induce LECs into collecting vessel phenotypes *in vitro.*[14,15,33–37] Thus, many mechanosensors and mechanotransduction pathways necessary for lymphatic collecting vessel development and maintenance in LECs have now been identified and explored for characterization.[14,15,33–41] In particular, the expression of key lymphatic vessel formation and maintenance transcription factors, such as FOXC2 and PROX1, differs in leaflet valve LECs compared with sinus LECs found within the collecting vessels[33,35,37,40](Figure 1A). This is a result of the shear stress levels being higher at the leaflet region than in the sinus region, though they both experience the oscillatory flow.[42] Another mechanosensor is the adherens junction proteins VE-cadherin (VE-CAD), which regulates lymphatic cell alignment and junctional integrity both *in vivo* and *in vitro* in response to shear stress for lymphatic vessel development and maintenance in collecting vessel LECs.[33,35,43–45] Other mechanosensitive cellular properties of LECs, such as proliferation and alignment, have also been described within the collecting vessels.[33,35,37,46,47] Though there is a growing interest in detailing lymphatic collecting vessel development, there is also the potential to use OSS as a biomechanical cue to engineer and mature LECs into a functional collecting vessels.

Here, we describe a method to induce a collecting vessel phenotype in LECs *in vitro* by introducing both physiological flow and synthetic HA to the cells. Based on previous *in vivo* and *in vitro* studies,[37,42,48–53] two OSS rates (0.5 and 10 dyn/cm^2) were used to stimulate the differing regions in the collecting vessel in these cells (Figure 1). We utilized our previously described synthetic dopamine-conjugated HA (HA-DP) coating to synergistically influence and maintain the lymphatic collecting vessel phenotype by reducing focal adhesion kinases (FAKs) and cytosol/cytoplasm F-actin fibers (confirmed in this study in static conditions), which result in the cytoplasmic degradation of YAP/TAZ that enhances PROX1 and its targets, thus preserving LEC characteristics and phenotypes.[24] We specifically used HA-DP at a degree of substitution value of 47% for its optimal usage of an *in vitro* coating and HA-binding site availability[24] (Figure S1). By investigating the effects of each stimulus individually and in combination, we report that OSS and HA interaction induces a lymphatic collecting vessel phenotype in the cultured LECs. We demonstrated that compared with the LECs cultured on FN (FN-LECs), the LECs cultured on HA-DP (HA-DP-LECs) exhibited an increase in their mechanotransduction activity in the presence of OSS and displayed mechanosensitive *in vivo* lymphatic collecting vessel properties.

RESULTS

HA-DP enhances lymphatic valve and sinus morphological characteristics

The presence of OSS *in vitro* has been demonstrated to influence the morphological response in LECs to a more cuboidal shape, which is similar to lymphatic valve-forming cells *in vivo.*[33] Surrounding lymphangion cells have been found to be more squamous.[33] On the basis of previous findings that demonstrated mechanotransduction differences between ECM

Please cite this article in press as: Lightsey et al., Engineering lymphatic collecting vessel phenotypes through combined hyaluronic acid cues and oscillatory shear stress, Cell Reports Methods (2026), https://doi.org/10.1016/j.crmeth.2026.101574

CellPress
OPEN ACCESS

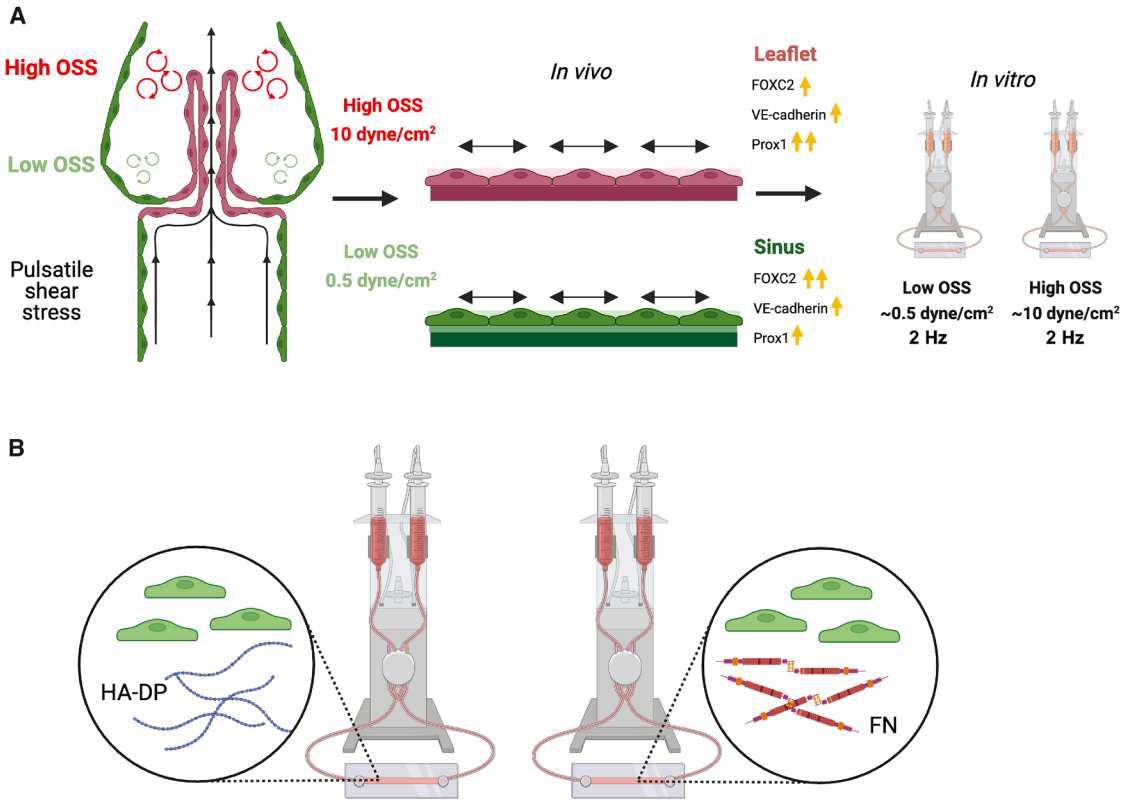

Figure 1. Physiological OSS in the valve region of lymphatic collecting vessels

(A) The sinus and leaflet regions of the lymphatic valve in the collecting vessel experience different rates of oscillatory shear stress (OSS). In these identified regions, LECs exhibit differential expression of key lymphatic mechanotransduction markers (PROX1, FOXC2, and VE-CAD). LECs have been found to alter and partially mimic these mechanotransduction responses *in vitro*.

(B) Using the ibidi pump system, HA-DP and FN coatings were used to investigate *in vitro* OSS behavior and compare the resulting LEC phenotypes. Schematic was created with BioRender.com.

components,[23,24,54–56] we investigated whether the HA-DP coating would alter lymphatic cell morphological characteristics that occur in response to OSS. We demonstrated that the HA-DP-LECs had significant changes in the cellular membrane shape distribution compared with the FN-LECs (Figure 2A). The average shape of individual cells in the population became either less circular (i.e., more irregular) or less round (i.e., decreased aspect ratio) in all conditions (Figure 2B). To confirm elongation changes, we also analyzed the nuclei of the corresponding cells. These morphological characteristics can be seen as early as 6 h after OSS (Figure S2). The circularity and roundness of the nuclear shapes were found to be significantly increased or decreased with the HA-DP coating compared to the FN-LECs at static and high-OSS conditions, while also showing OSS-dependent changes at low OSS that were not seen in FN-LECs (Figure 2C). These changes in shape descriptors show that the HA-DP coating influenced a more irregular morphology across all conditions. Altogether, we observed that static HA-DP-LECs became more irregular, low-OSS HA-DP-LECs had a more elongated cell membrane (a typical characteristic of squamous sinus LECs[33]), and high-OSS HA-DP-LECs were increasingly cuboidal (a feature of lymphatic valve-forming LECs[33]), as observed from their more circular nuclei but less round membranes (Figure 2D). To confirm the collecting vessel morphology, the VE-CAD membrane was assessed to determine the presence of "zipper-like" structures between the cells (Figure S3). We observed an increase in continuous junction membrane thickness in HA-DP-LECs compared with the FN-LECs (Figure 2E) as well as increased slab and voxel junction branching in the cell membranes (Figure 2F) that are characteristic of "zipper-like" junctions.[44,57,58] Thus, the HA-DP coating altered the morphological responses of LECs in the presence of OSS to become increasingly like their corresponding *in vivo* collecting vessel leaflet and sinus LECs.

HA-DP induces cytoskeleton distribution and activates perinuclear and cytoplasmic F-actin

F-actin distribution between the static and OSS conditions have been found to be similar *in vitro*, while F-actin activation and localization in LECs have been found to be altered under *in vitro* static and flow conditions as well as within different areas of the developing lymphatic valve *in vivo*.[33,59] We then investigated the F-actin directionality, intensity, and localization properties between HA-DP-LECs and FN-LECs under static, low-OSS, and high-OSS conditions. We observed cytoskeleton differences between FN-LECs and HA-DP-LECs

Please cite this article in press as: Lightsey et al., Engineering lymphatic collecting vessel phenotypes through combined hyaluronic acid cues and oscillatory shear stress, Cell Reports Methods (2026), https://doi.org/10.1016/j.crmeth.2026.101574

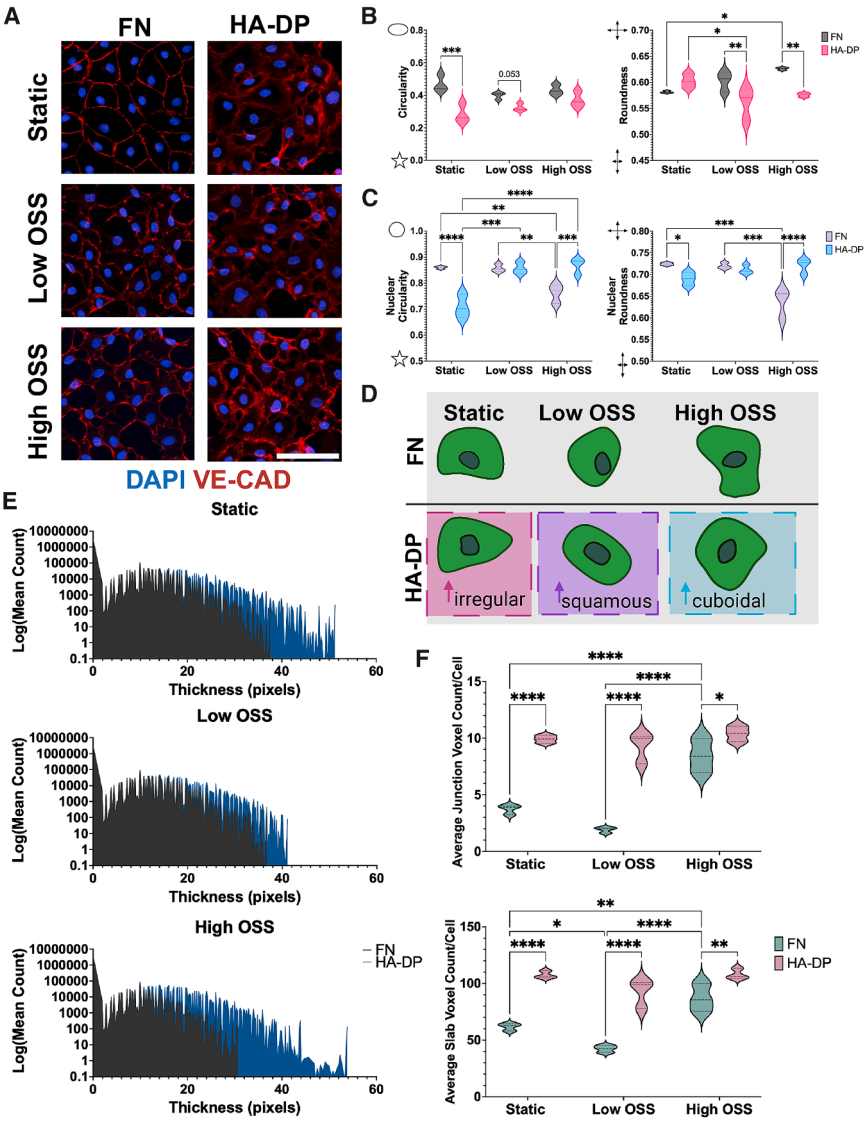

Figure 2. Collecting vessel morphology is confirmed and enhanced in HA-DP-LECs, especially under OSS

(A) VE-CAD (red) staining in HA-DP-coated slides demonstrated an increase in the morphological response of LECs to varying OSS rates to either a more cuboidal shape (at low OSS) or more squamous shape (at high OSS) compared with the FN coating. Scale bars: 100 μm.

(B) Circularity and roundness of LEC membranes under static and OSS conditions.

(C) Nuclear circularity and nuclear roundness of LECs under static and OSS conditions. Circularity values: 1, perfect circle; 0, irregular shape. Roundness values: 1, more circular. Data represent the mean ± SD, with $n = 3$ slides per condition (three images per slide and >70 cells per image).

(D) Graphical summary of the morphological differences between FN and HA-DP LECs. Created in BioRender.com.

(E) Average VE-CAD membrane thickness (pixels) across $n = 3$ slides (three images per slide).

(F) Average junction voxel and slab voxel counts per cell. Data represent the mean ± SD, with $n = 3$ slides per condition (three images per slide).

Two-way ANOVA was performed with a Tukey's multiple-comparison test. Significance levels were set at $^{*}p < 0.5$, $^{**}p < 0.01$, $^{***}p < 0.001$, and $^{****}p < 0.0001$.

under static and OSS conditions (Figure 3A). Quantitative analysis and normalization demonstrated that both FN and HA-DP similarly distribute the cytoskeleton in 0°–90° directionalities in the presence of OSS (Figure 3B). There was also no significant change in confluency across all conditions (even at a different concentration of FN), and confluency changes occurred only between 0 and 48 h of shear stress after slides reached confluency (Figure S4). At higher magnifications, the nuclear F-actin intensity in HA-DP-LECs was higher than that in FN-LECs in OSS conditions (Figures 3C and 3D). These findings can be associated with enhanced mechanotransduction signaling and elevated mechanical responses.[33,47,60,61] We then observed that the perinuclear intensity in HA-DP-LECs was decreased in static and low-OSS conditions but increased in high-OSS conditions compared with FN-LECs (Figures 3C and 3E). HA-DP influenced a more responsive biomimetic accumulation of perinuclear F-actin high-OSS ("leaflet like") conditions[33,55,62] when compared with FN-LECs. In the cytoplasmic region, low-OSS HA-DP-LECs had a decrease in intensity, but the overall intensity trends between the static and shear stress levels remained the same between HA-DP-LECs and FN-LECs (Figure 3F). To assess the trends further, ratios between F-actin localization regions were determined to quantify cytoskeleton organization (Figures 3G–3I). We found that static HA-DP-LECs had a higher nuclear/perinuclear ratio and no change in the other ratios compared with FN-LECs, thus demonstrating an expected accumulation of cytoplasmic F-actin[33,55,62] and an increased localization in the nuclei (Figures 3G–3I). Low-OSS HA-DP-LECs had an increased perinuclear/cytoplasm, nuclear/cytoplasm, and nuclear/perinuclear localization of F-actin compared with FN-LECs, thus confirming reduced cytosol F-actin, which is a characteristic of cortical F-actin found in squamous collecting vessel LECs.[33,35,58] High-OSS HA-DP-LECs ratios remained the same but showed a significant decrease compared with low-OSS HA-DP-LECs in terms of all ratios (unlike FN-LECs) (Figures 3G–3I). This demonstrates that the shear-stress-dependent mechanotransduction signaling is not negatively impacted by HA-DP and that there is an enhanced mechanical response in HA-DP-LECs under OSS. These findings demonstrate that HA-DP-LECs are responsible for reorganizing and distributing the cytoskeleton properly in response to OSS, while also further activating certain localized filaments.

Please cite this article in press as: Lightsey et al., Engineering lymphatic collecting vessel phenotypes through combined hyaluronic acid cues and oscillatory shear stress, Cell Reports Methods (2026), https://doi.org/10.1016/j.crmeth.2026.101574

CellPress
OPEN ACCESS

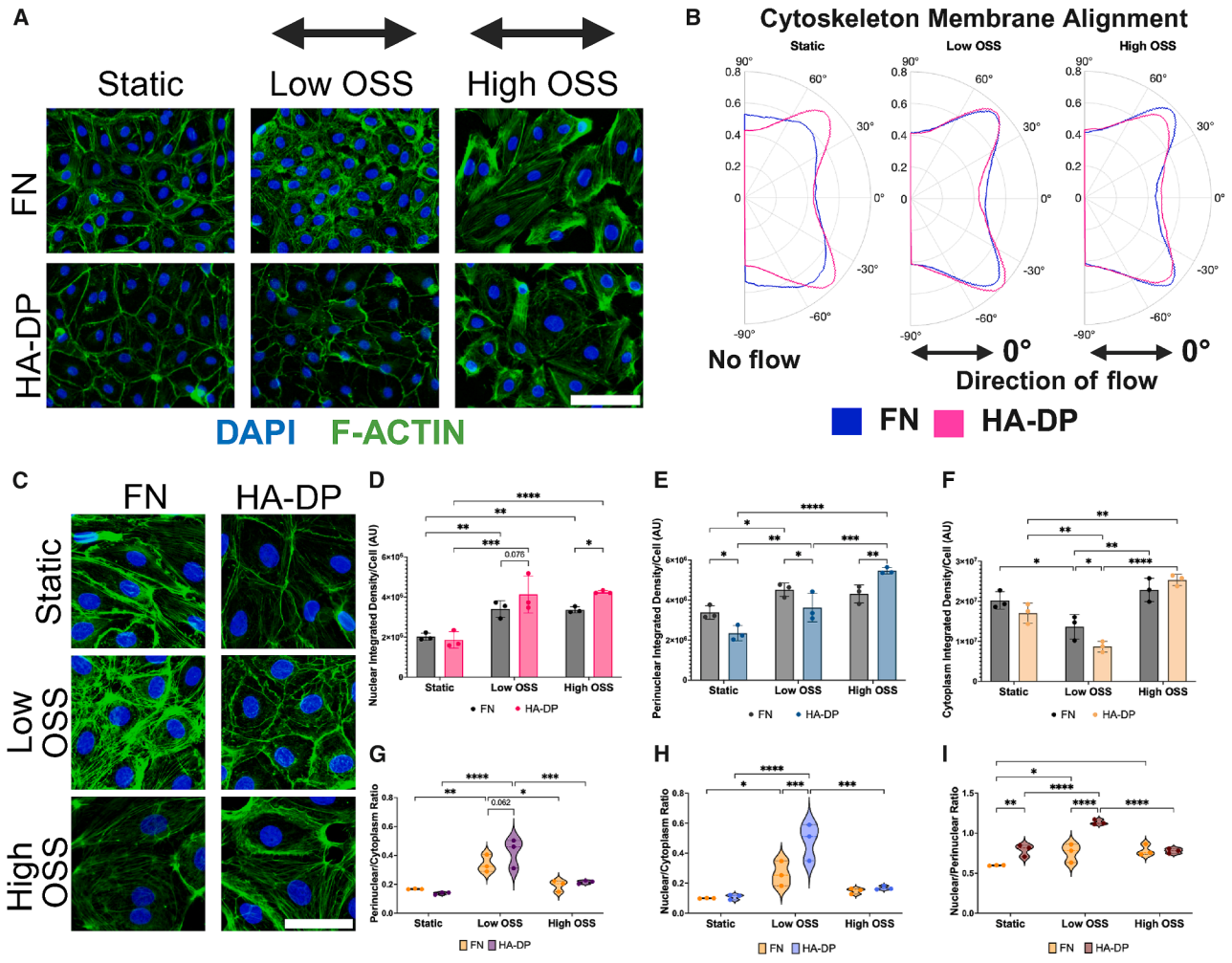

Figure 3. HA-DP-LECs induce cytoskeleton distribution and provide more prominent OSS-related F-actin responses

(A) F-actin in LECs demonstrates alignment changes based on OSS and coating. Scale bars represent 100 μm.

(B) Average percent distribution of the directionality of LECs. Mean of $n = 3$ slides per condition (three images per slide and >90 cells per image).

(C–I) Nuclear, perinuclear, and cytoplasm F-actin localization and distribution of LECs. Scale bars: 50 μm. Integrated density per cell at (D) nuclear, (E) perinuclear, and (F) cytoplasm location with (G) perinuclear/cytoplasm ratio, (H) nuclear/cytoplasm ratio, and (I) nuclear/perinuclear ratio. Data represent the mean ± SD, with $n = 3$ slides per condition (three images per slide and >30 cells per image). Two-way ANOVA was performed with a Tukey's multiple-comparison test. Significance levels were set at $^{*}p < 0.5$, $^{**}p < 0.01$, $^{***}p < 0.001$, and $^{****}p < 0.0001$.

HA-DP amplifies mechanotransduction responses in LECs in response to varying OSS rates

Lymphangiogenesis is characterized by a high number of markers and pathways, which include mechanotransduction pathways.[14,15,33,34,36–41,43,44] The expression of key lymphatic valve formation and maintenance transcription factors, such as FOXC2 and PROX1, differs in leaflet valve LECs compared with collecting vessel LECs found in the sinus region.[33,35,37,40,42,45] To investigate the lymphatic collecting vessel phenotype, PROX1, FOXC2, and VE-CAD were immunofluorescence stained and quantified (Figure 4A). Protein intensity quantification demonstrated that there were significant changes in HA-DP-LECs in the presence of OSS (Figures 4B–4D). Though nuclear PROX1 remained consistent between HA-DP-LECs, VE-CAD increased and FOXC2 decreased at high OSS with HA-DP. These elevated markers are characteristic of LECs in collecting vessels in the presence of OSS.[37,43,45] The decrease in PROX1 at high OSS for both FN-LECs and HA-DP-LECs is expected, as this frequent rate can cause LEC damage and is associated with *in vivo* PROX1^{low} populations in the collecting vessel.[33,37] However, we did observe enhanced PROX1 and FOXC2 nuclear localization in HA-DP-LECs at all OSS rates (Figures 4E and 4F), demonstrating the HA-DP enhancement of gene regulation and activity. To further confirm the collecting vessel phenotype, we assessed PDPN and LYVE-1 expression in all conditions. We found that PDPN in HA-DP-LECs decreased in response to all OSS conditions, unlike FN-LECs, and was significantly less expressed in OSS conditions compared with FN-LECs (Figures 4G and 4H). LYVE-1 expression was decreased in response to OSS in HA-DP-LECs and FN-LECs, with HA-DP-LECs having comparatively

Please cite this article in press as: Lightsey et al., Engineering lymphatic collecting vessel phenotypes through combined hyaluronic acid cues and oscillatory shear stress, Cell Reports Methods (2026), https://doi.org/10.1016/j.crmeth.2026.101574

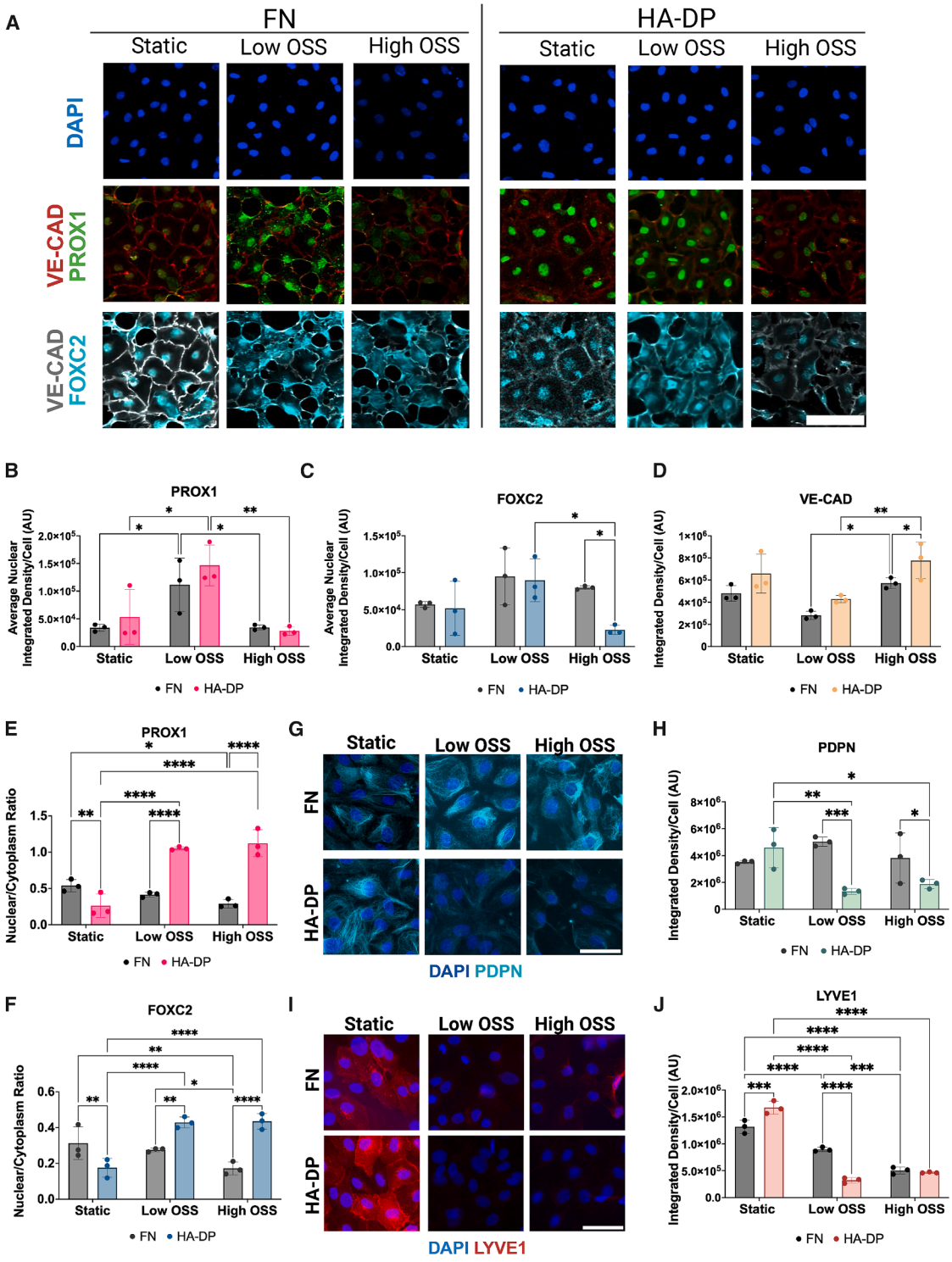

Figure 4. Key lymphatic mechanotransduction markers are more efficiently localized while key lymphatic capillary markers are decreased in HA-DP-LECs under OSS

(A–D) Expressions of primary mechanosensitive lymphatic markers (PROX1, FOXC2, and VE-CAD) were investigated and quantified in FN-LECs and HA-DP-LECs.

(E and F) Nuclear localization of PROX1 (E) and FOXC2 (F) was measured from immunofluorescent images. Scale bars: 100 μm. Data represent the mean ± SD, with n = 3 slides per condition (three images per slide and >400 cells per image).

(legend continued on next page)

Please cite this article in press as: Lightsey et al., Engineering lymphatic collecting vessel phenotypes through combined hyaluronic acid cues and oscillatory shear stress, Cell Reports Methods (2026), https://doi.org/10.1016/j.crmeth.2026.101574

higher LYVE-1 in static conditions and lower LYVE-1 in low-OSS conditions (Figures 4I and 4J). This PDPN^{low}/LYVE-1^{low} phenotype in HA-DP-LECs are characteristic of the collecting vessel LECs.[35,37,40,63]

To further assess these pathways in the presence of OSS and with HA-DP coating, a pre-formatted PCR array panel with markers and targets for angiogenesis and lymphangiogenesis was used to analyze and detect genes present in these slides. Heatmaps between both HA-DP-LECs and FN-LECs demonstrated that there was a change in angiogenic and lymphangiogenic gene expressions at static and all OSS rates (Figure 5A). Furthermore, volcano plots of HA-DP-LECs and FN-LECs under OSS compared with static FN-LECs demonstrated that HA-DP-LECs underwent greater fold changes in markers (Figure 5B). Key collecting vessel lymphatic markers also appeared to be altered with the HA-DP coating, with an overall increase in *PROX1* and *CDH5* (i.e., genes encoding VE-CAD) in HA-DP-LECs under all static and OSS conditions (Figures 5C and 5E). *FOXC2* expression between the HA-DP-LECs and FN-LECs followed the trend seen at the protein level (Figure 5D). *LYVE-1* expression in FN-LECs and HA-DP-LECs was similar to its protein expression trends, which confirmed the elevated LYVE-1/HA interaction in static HA-DP-LECs and its downregulation in OSS conditions (Figure 5F), essential for the lymphatic collecting vessel.[64] Interestingly, HA-DP-LECs showed reduced *VEGF-C* expression in all conditions, while FN-LECs had decreased *VEGF-C* only in OSS conditions (Figure 5G). Other relevant markers, such as *VEGFR2* and *CTGF* (i.e., YAP/TAZ downstream marker), confirmed the general lymphatic identity preservation in static HA-DP-LECs and/or also showed an increased collecting vessel phenotype in OSS conditions (Figure S5). These findings demonstrate that the HA-DP-LECs either similarly induce or enhance mechanotransduction responses found in the collecting vessel in the presence of varying OSS rates.

Proliferation activity and mTORC1 mechanotransduction activity enhanced in HA-DP-LECs

In vivo proliferation profiles show that the collecting vessel LECs undergo greater proliferation than the capillary vessel LECs and that the highest proliferative LEC population is found in the valve area (especially sinus region) to maintain valve integrity.[35,37,46] To investigate any differences in the proliferation activity, the cells were immunofluorescence stained with Ki67 after OSS exposure. We confirmed the Ki67$^+$ percentage trends in FN-LECs (Figures 6A and 6B), as depicted in previous studies.[37] However, we found that HA-DP-LECs has a significantly increased Ki67$^+$ percentage at high OSS, which is characteristic of the collecting vessel phenotype, while FN-LECs under high OSS had a lower Ki67$^+$ percentage (Figure 6B). At low OSS, the HA-DP-LECs also had increased Ki67$^+$ compared with static HA-DP-LECs, a characteristic of sinus LECs. While the proliferation activity was similar between HA-DP-LECs and FN-LECs in the static and low OSS conditions, the maintenance of proliferation activity in HA-DP-LECs in OSS conditions was found in the collecting vessels but not seen in FN-LECs (Figure 6B).

It has been recently found that mTORC1 signaling is a mechanosensitive pathway that is essential for lymphatic collecting vessel development and maintenance, specifically for the cell proliferation profiles and durability of valve (leaflet and sinus) LECs.[45,65–67] To confirm the maintained presence of shear stress level-dependent mechanotransduction processes in HA-DP-LECs, all conditions were treated with rapamycin (a pharmacological inhibitor of mTORC1) to confirm the loss of collecting vessel phenotypes, including mTORC1 activity, lymphatic cell identity, and proliferation behavior, which were similar between the HA-DP-LECs and FN-LECs. Using phosphorylated S6 (pS6) ribosomal protein (Ser240/244) to determine the levels of mTORC1 activity,[37,68] we demonstrated that the average pS6 intensity was similarly increased only at high OSS in both HA-DP-LECs and FN-LECs treated with rapamycin (Figures 6C and 6D). However, HA-DP-LECs showed a significantly lower level of pS6 at high OSS than the FN-LECs under rapamycin treatment (Figure 6D). Similarly, rapamycin-treated HA-DP-LECs and FN-LECs had a comparable average PROX1 intensity under static and low-OSS conditions, but HA-DP-LECs under high OSS had significantly lower PROX1 intensity than the FN-LECs under high OSS (Figures 6E and 6F). Interestingly, the Ki67$^+$ percentages between the HA-DP-LECs and FN-LECs treated with rapamycin under static and OSS conditions remained insignificant and showed no differences (Figure S6). Thus, we show that HA-DP-LECs can maintain and/or increase the inhibition of mTORC1 in the presence of rapamycin during static and OSS conditions, which suggests its mechanistic reliance on the mechanosignaling pathways.

DISCUSSION

LECs are mechanoresponsive to either laminar or oscillatory flow both *in vivo* and *in vitro*. To model lymphatic developmental biology, *in vitro* OSS has been previously used to achieve the phenotypes found within the lymphatic system, particularly the lymphatic collecting vessel.[33–36,45,55,69,70] However, there has been limited findings on how *in vitro* OSS can mechanically induce LECs for lymphatic tissue engineering purposes.[49,56,71–73] Furthermore, previous studies have performed *in vitro* OSS in LECs that have been coated with FN due to its required interaction with integrin-α9 on LECs for lymphatic valve morphogenesis.[22,39] By investigating the OSS-induced mechanotransduction responses in LECs on another promising ECM material (HA), we report a method to better induce the lymphatic collecting vessel phenotype in cultured LECs via the HA-LYVE-1 interaction.

Morphological and cytoskeleton alterations in LECs are the key indicators of mechanotransduction signaling, especially in response to oscillatory flow.[14,17,33,35,47,59,74,75] These alterations are also present *in vivo*, specifically in differing areas of the

(G–J) Lymphatic capillary markers were investigated and quantified, specifically (G and H) PDPN and (I and J) LYVE-1. Scale bars: 50 μm. Data represent the mean ± SD, with $n = 3$ slides per condition (three images per slide and >90 cells per image). Two-way ANOVA was performed with a Tukey's multiple-comparison test.

Significance levels were set at $^*p < 0.5$, $^{**}p < 0.01$, $^{***}p < 0.001$, and $^{****}p < 0.0001$.

CellPress
OPEN ACCESS

Cell Reports Methods
Article

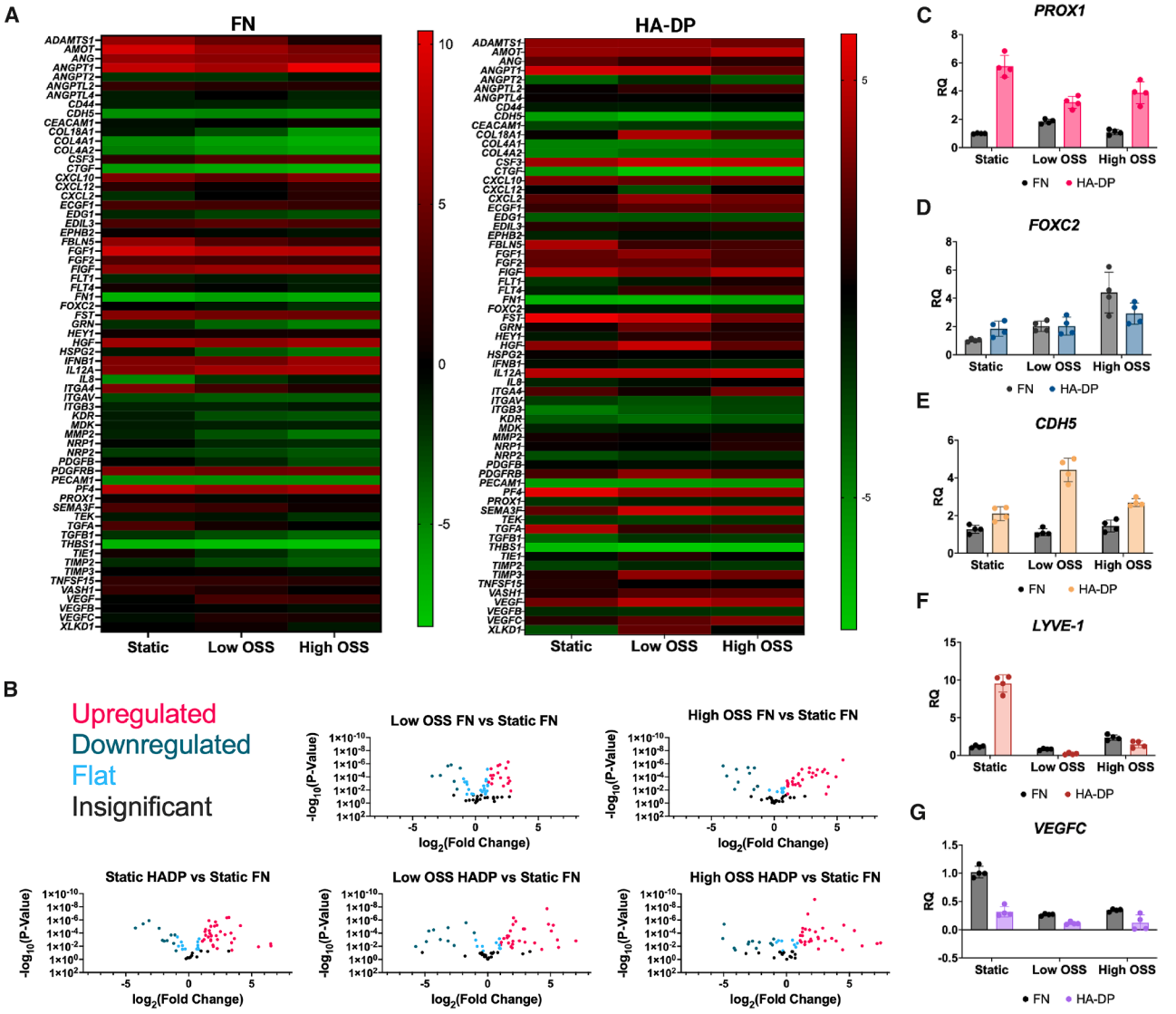

Figure 5. HA-DP and OSS influence the regulation of lymphangiogenesis genes that are mechanosensitive in LECs

(A) Heatmap of human angiogenesis PCR panel between FN and HA-DP LECs across varying OSS rates confirms differing mechanotransduction responses.

(B) Volcano plots of all conditions compared with static FN, using a Student's *t* test with the specified group. Significant boundary of *p* value is at 0.05, and fold change boundary is at 2.

(C–G) Key collecting vessel/identity lymphatic markers, *PROX1* (C), *FOXC2* (D), *CDH5* (E), *LYVE-1* (F), and *VEGF-C* (G) demonstrate OSS- and coating-dependent alterations in respective genetic expressions. Data represent the mean ± SEM of $n = 3$ pooled slides.

collecting vessel.[33] The use of HA-DP with LECs under static and OSS conditions provided an alternate biomechanical stimulation that improved the distribution of cellular shapes to more similarly reflect corresponding *in vivo* characteristics[33] (i.e., increasingly elongated at static, increasingly cuboidal at low OSS, and increasingly squamous at high OSS). In our previous study describing the interaction between LECs and HA-DP, we found that the expression of FAKs and F-actin stress fibers decreased, thus leading to the conclusion that there is less mechanotransduction signaling compared with fibronectin in static conditions.[24] However, our detailed findings on F-actin distribution and increased localized intensity trends in static and OSS HA-DP-LECs, compared with FN-LECs, demonstrate the significant presence of the mechanotransduction signaling properties from HA-DP. Furthermore, the OSS-dependent changes in F-actin localization, intensity, and ratios in HA-DP-LECs are more consistent with *in vivo* F-actin characteristics of collecting vessels.[33,55,62] HA-DP provides an increasingly biomimetic 2D environment for cytoskeleton arrangement, especially in the presence of OSS, which is crucial for understanding collecting vessel development. These conclusions are also consistent with the previous findings of HA-LYVE-1 interactions on LECs being dependent on cytoskeleton actin arrangement and distribution.[76]

Please cite this article in press as: Lightsey et al., Engineering lymphatic collecting vessel phenotypes through combined hyaluronic acid cues and oscillatory shear stress, Cell Reports Methods (2026), https://doi.org/10.1016/j.crmeth.2026.101574

CellPress
OPEN ACCESS

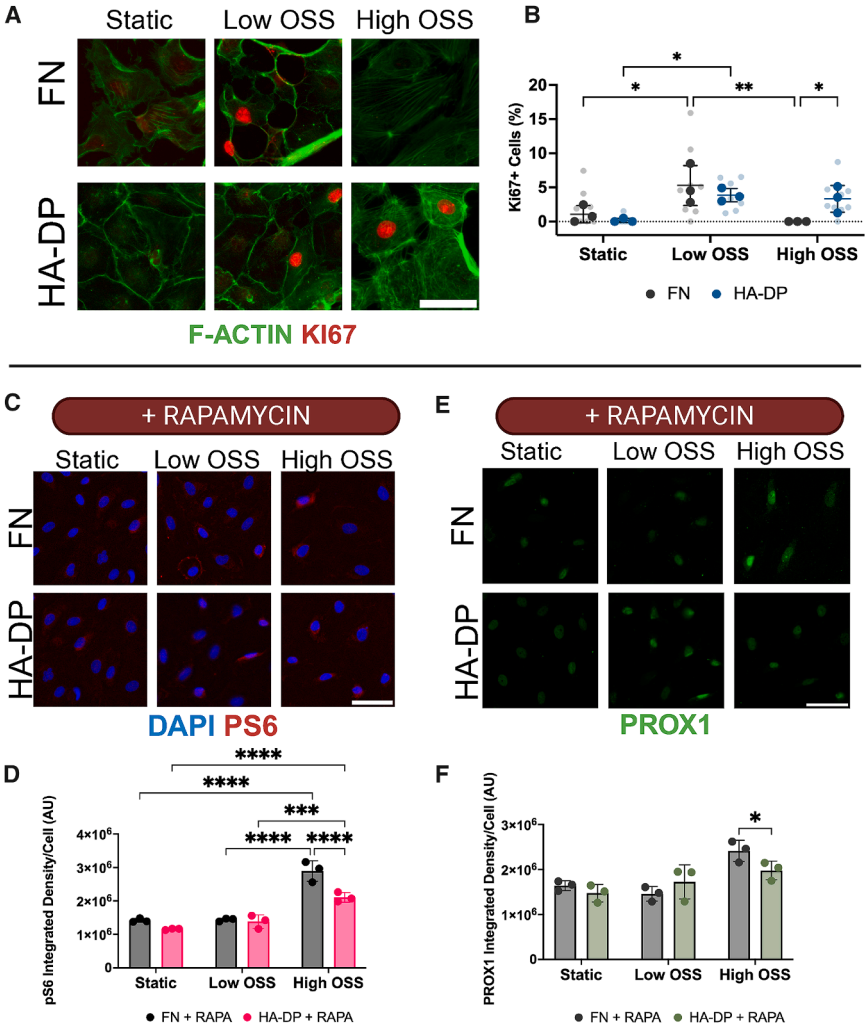

Figure 6. mTORC1 mechanotransduction regulation and proliferation activity enhanced in HA-DP-LECs under OSS

(A) F-actin and Ki67 staining show increased proliferation in HA-DP LECs at low and high OSS rates compared with its static condition.

(B) Quantitative results of Ki67^{+} cells. Data represent the mean ± SD of n = 3 slides per condition (three images and >90 cells per slide).

(C and D) pS6 staining in rapamycin-treated LECs in all conditions (C), and quantification of images shows enhancement of inhibition with HA-DP at high OSS (D).

(E and F) PROX1 staining in rapamycin-treated LECs in all conditions (E), and quantification of images shows similar inhibition patterns (F).

Scale bars are 50 μm. Data represent the mean ± SD of n = 3 slides per condition (four images and >60 cells per slide). Two-way ANOVA was performed with a Tukey's multiple-comparison test. Significance levels were set at $^{*}p < 0.5$, $^{**}p < 0.01$,$^{***}p < 0.001$, and $^{****}p < 0.0001$.

Mechanosensing pathways that are responsive to OSS in LECs lead to mechanotransduction pathways that control important lymphangiogenesis responses, including collecting vessel development.[14,15,33–41] PROX1 is required for mechanotransduction signaling in response to flow and is an important regulator of lymphatic development.[14,33,35,59,64] FOXC2 is upregulated in collecting vessel LECs in response to flow and is the key marker responsible for the maturation and development of lymphatic valves.[33,35,40,45,77] VE-CAD is also upregulated in lymphatic valve LECs in response to flow and plays a role in OSS mechanotransduction signaling (including regulating expression of PROX1 and FOXC2) for lymphatic collecting vessel development and maintenance.[35,43,44] In response to physiological OSS flow rates, we found that HA-DP-LECs tend to experience rate-dependent expressions of PROX1, FOXC2, and VE-CAD, which are essential characteristics for collecting vessel LECs. We also found that the genetic expression of key regulator markers may vary between shear stress levels and coatings (FN and HA-DP), thus demonstrating the possible role of post-translational modifications[34,78] and/or translational regulation mechanisms[79,80] when LECs are exposed to OSS. PROX1 is elevated in the lymphatic valve *in vivo*,[33,35,40,45] which was confirmed in the protein quantification of both FN-LECs and HA-DP-LECs exposed to low OSS (Figure 4B). *PROX1* expression was found to be generally increased in HA-DP-LECs at all rates compared with FN-LECs and its protein expression (Figure 5C). Though previous studies with FN-LECs have not found *in vitro* OSS-dependent increases in PROX1,[33,34,43,81] evidence from this study suggests that the introduction of a higher frequency shear (~2 Hz) in an oscillatory laminar flow replicates and/or enhances previous *in vitro* lymphatic collecting vessel FN-LEC phenotypes. The higher frequency was conducted to provide an increasingly biomimetic environment (i.e., similar to OSS/disturbed flow) that experiences increased inertial forces (Womersley number above 2; Figure S7)[16,33,42,48,82,83] related to oscillations, while still maintaining an overall viscous dominated flow (Reynolds number at ~0.12). Furthermore, collecting vessel and lymphatic valve LECs experience increased expression of FOXC2 compared with capillary LECs, with the highest expression of FOXC2 being located in the sinus area of the lymphatic valve that is usually in the presence of low recirculating flow (<1 dyne/cm^2).[14,33,35] Though *FOXC2* expression was relatively indifferent between most conditions (Figure 5D), the FOXC2 expression was elevated under low OSS and decreased under high OSS in HA-DP-LECs, while those in FN-LECs remained unchanged under high OSS (Figure 4C). Nuclear localization of PROX1 and FOXC2 increased significantly in response to OSS in HA-DP-LECs, thus signifying increased signaling and marker activity.[84] *CDH5* expression was elevated and OSS rate dependent in HA-DP-LECs across all conditions compared

Please cite this article in press as: Lightsey et al., Engineering lymphatic collecting vessel phenotypes through combined hyaluronic acid cues and oscillatory shear stress, Cell Reports Methods (2026), https://doi.org/10.1016/j.crmeth.2026.101574

with FN-LECs (Figure 5E), with VE-CAD expression being OSS dependent and elevated as well (Figure 4D). Furthermore, HA-DP-LECs expressed less PDPN compared with FN in all OSS conditions and less LYVE-1 in low-OSS conditions (Figures 4H and 4J). These changes in key lymphatic and mechanotransduction markers signify the influence of HA-DP in LECs under OSS and its ability to manipulate the biomechanical behavior. The PCR array demonstrated the increased trends in fold changes in HA-DP-LECs compared with FN-LECs under static and OSS conditions, which further displays the influential capabilities of HA-DP (Figures 5A and B). Furthermore, the characteristic expression of lymphatic collecting vessel-related markers across all conditions in HA-DP-LECs demonstrated and confirmed that HA-DP can heavily influence the LEC mechanotransduction signaling and pathways (Figures 5C–G).

To further confirm the stronger mechanotransduction influence of HA-DP in OSS responses in LECs compared with FN, we investigated the proliferation activity, as its importance in lymphatic collecting vessel development and maintenance as well as its dependence on OSS rates has been recently identified and highlighted.[33,35,37,42,85] The escalator model, proposed and confirmed by Saygili Demir et al.,[37] illustrates that sinus LECs that are exposed to low OSS tend to increase their proliferation activity to replace the leaflet LECs that are exposed to high OSS due to damage and low proliferation activity. The *in vitro* findings in Saygili Demir et al. were confirmed with the FN-LECs (Figure 6B) under the selected low- and high-OSS rates in this study. However, HA-DP-LECs demonstrated similar increases in the proliferation activity during both low and high OSS compared with static conditions (Figure 6B), thus confirming the change in mTORC1 signaling, which is mechanosensitive to OSS and differing shear stress levels. Though not following previous models, the increased proliferative activity in HA-DP-LECs under OSS compared with static conditions is characteristic of collecting vessel LECs compared with capillary vessel LECs[35,37,46] which distinguishes the HA-DP-LECs.

The mechanosensitive role of mTORC1 signaling in LECs exposed to shear stress during lymphatic collecting vessel development has recently been highlighted to be necessary for proper mechanotransduction pathway responses.[37,45,46,65–67] The use of rapamycin inhibits the function of mTORC1 and has been found to most significantly impact the proliferative response of LECs to low shear stress.[37] It has also been found that rapamycin can inhibit LEC proliferation and PROX1 expression in static conditions.[46,65] We report that HA-DP-LECs demonstrated similar or further inhibition of mTORC1 when treated with rapamycin depending on the shear stress condition, which confirms its mechanotransduction dependence on the critical mTORC1 pathway and increased mechanosignaling activity compared with FN-LECs. Notably, the decreased pS6 and PROX1 expression at high OSS in HA-DP-LECs (Figures 6D and 6F) provides mechanistical insight that suggests an increased dependence on the mTORC1 pathway, which is likely due to its role in regulating PROX1[65] and the confirmed behavior of HA-DP on key lymphatic markers in static and OSS conditions.

Most studies have utilized FN as a coating to study the mechanotransduction processes related to lymphatic collecting vessel development in LECs when they are exposed to 2D shear stress.[33–35,37,40,45,47,86] However, the engineering of a 3D collecting lymphatic vessel requires the use of a biomaterial-based hydrogel that is tunable and can be manipulated both chemically and mechanically to ensure that lymphangiogenesis occurs properly and is reproducible. As demonstrated in previous studies,[4,7,9,13,23,49,55,71–73,87] the ideal hydrogels for facilitating *in vivo* and *in vitro* lymphangiogenesis are synthetic and need to be validated once introduced to increased mechanical forces (i.e., flow). Recent microfluidic models that incorporate the biomechanical forces in the valve morphology, such as the thrombosis-on-a-chip platform[88] and vein-chip platform,[89] also require incorporating lymphatic-related ECM biomaterials to enhance the lymphatic collecting vessel phenotype. By using our synthetic HA-based coating and comparing it to FN coating, we report that LECs can synergistically enhance their mechanotransduction activity that is found *in vivo* when they're developing into collecting vessel LECs (Figure 7). We demonstrated that the combinational use of a biomechanical (OSS) and biochemical (HA-DP) stimuli can induce increased collecting vessel-related lymphangiogenesis in LECs. These findings confirm the mechanotransduction properties of LECs and the complexity of their ECM interactions to inspire future directions of engineering 3D collecting lymphatic vessels. Furthermore, it provides potential mechanistic pathways (i.e., LYVE-1, PROX1, etc.) to be explored in LECs when they are exposed to shear stress. Overall, HA and OSS are viable mechanisms to explore the *in vitro* 2D and 3D culturing of collecting vessel LECs.

Limitations of the study

While our study demonstrates the significance of the HA and LEC interaction in the presence of *in vitro* OSS, the precise characterization of the disturbed and recirculatory flow found *in vivo* is difficult to model *in vitro*,[20,42,49] which can perturb the expected *in vivo* LEC behavior. To ensure a representative and accurate model, we have utilized a previously defined and validated *in vitro* shear stress model,[33,37] while also increasing the frequency to stimulate a more disturbed flow compared with previous models (as described above). Though many 2D *in vitro* models cannot precisely demonstrate *in vivo* flow patterns, we provide an insight into the methods to enhance LEC responses to those found *in vivo*. Furthermore, dermal LECs were utilized under flow, rather than using organ-specific LECs (i.e., intestinal LECs, etc.), which might have altered the previously established LEC/OSS behavior[33,35,37,45] due to potentially substantial differing roles of LECs in different organs.[57] However, dermal LECs have a highly similar marker expression profile and demonstrate similar lymphangiogenesis behavior to the intestinal LECs.[57,90,91] Dermal lymphatics are also commonly used in modeling lymphedema *in vitro* and *in vivo*.[4,92–94]

RESOURCE AVAILABILITY

Lead contact

Requests for further information and resources should be directed to and will be fulfilled by the lead contact, Donny Hanjaya-Putra (dputra1@nd.edu).

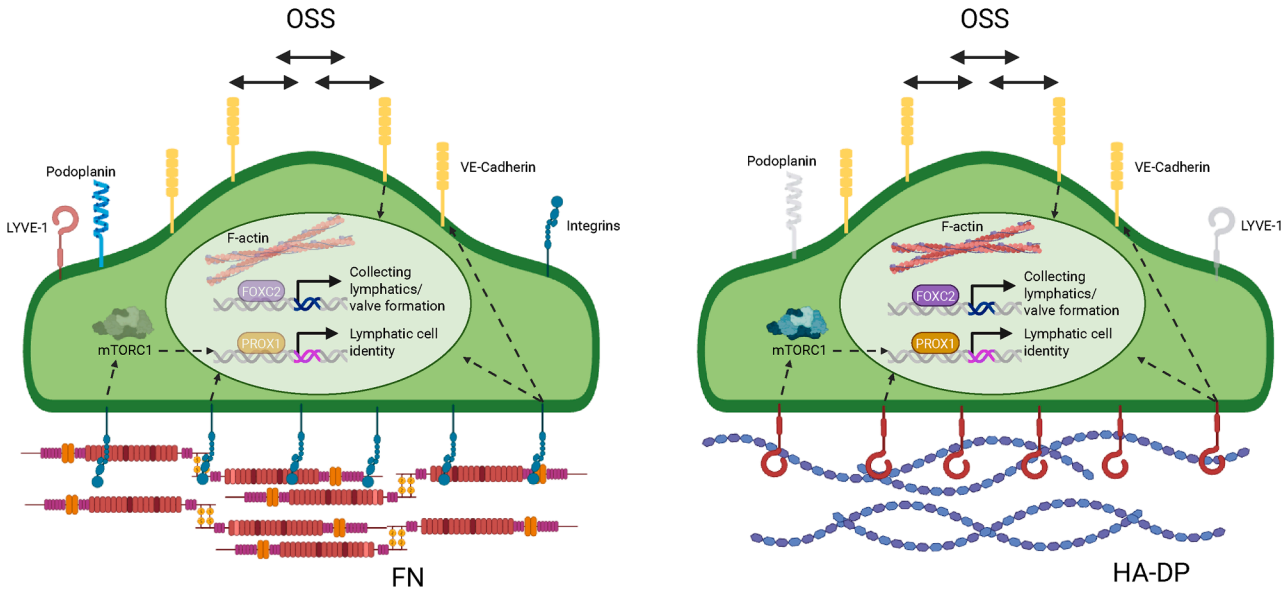

Figure 7. HA can enhance OSS mechanotransduction responses in LECs that are crucial to achieve a lymphatic collecting vessel phenotype
Compared with FN, the combination of the ECM protein, HA, and physiological flow can induce unique responses in essential mechanosignaling pathways including PROX1 and FOXC2 nuclear localization, nuclear F-actin activation, mTORC1 dependency, increased junctional activity, and PDPN and LYVE-1 reduction. HA-DP can be utilized to investigate the development of a 3D lymphatic collecting vessel and provide avenues for biomechanical exploration (i.e., LYVE-1 and PROX1). Schematic was created using BioRender.com.

Materials availability

This study did not generate new unique reagents.

Data and code availability

- Data reported in this paper will be shared by the lead contact upon request.
- This paper does not report original code.
- Any additional information required to reanalyze data reported in this work is available from the lead contact upon request.

ACKNOWLEDGMENTS

We acknowledge support from the University of Notre Dame through "Advancing Our Vision" Initiative in Stem Cell Research, Harper Cancer Research Institute – American Cancer Society Institutional Research grant (IRG-17-182-04), American Heart Association through Career Development award (19-CDA-34630012 to D.H.-P.), National Science Foundation (2047903 and 2225601 to D.H.-P.), National Institutes of Health (1R35-GM-143055 to D.H.-P.), and GEM fellowship to N.K.L.

AUTHOR CONTRIBUTIONS

N.K.L and D.H.-P. conceived the ideas, designed the experiments, interpreted the data, and wrote the manuscript. N.K.L, F.F., S.S., E.H., and D.H.-P. conceptualized the methodology. N.K.L., G.F., and B.C.-G. conducted the experiments and analyzed the data. All authors have approved the manuscript.

DECLARATION OF INTERESTS

This work has been disclosed to the IDEA Center at the University of Notre Dame. The synthetic HA dopamine coating has been filed for a provisional patent.

STAR★METHODS

Detailed methods are provided in the online version of this paper and include the following:

- KEY RESOURCES TABLE
- EXPERIMENTAL MODEL AND STUDY PARTICIPANT DETAILS
  - Cell source and culture
  - Cell culture under flow set up
- METHOD DETAILS
  - Dopamine-modified hyaluronic acid synthesis
  - Extracellular matrix coating
  - Immunofluorescent imaging
  - Gene expression
- QUANTIFICATION AND STATISTICAL ANALYSIS
  - Image analysis
  - Statistical analysis
- ADDITIONAL RESOURCES

SUPPLEMENTAL INFORMATION

Supplemental information can be found online at https://doi.org/10.1016/j.crmeth.2026.101574.

Received: October 10, 2025
Revised: May 25, 2026
Accepted: August 6, 2026

REFERENCES

1. Alderfer, L., Wei, A., and Hanjaya-Putra, D. (2018). Lymphatic Tissue Engineering and Regeneration. J. Biol. Eng. *12*, 32. https://doi.org/10.1186/s13036-018-0122-7.

2. Jia, W., Hitchcock-Szilagyi, H., He, W., Goldman, J., and Zhao, F. (2021). Engineering the Lymphatic Network: A Solution to Lymphedema. Adv. Healthcare Mater. *10*, 2001537. https://doi.org/10.1002/adhm.202001537.

3. Campbell, K.T., and Silva, E.A. (2020). Biomaterial Based Strategies for Engineering New Lymphatic Vasculature. Adv. Healthcare Mater. *9*, 2000895. https://doi.org/10.1002/adhm.202000895.

4. Hooks, J.S.T., Bernard, F.C., Cruz-Acuña, R., Nepiyushchikh, Z., Gonzalez-Vargas, Y., García, A.J., and Dixon, J.B. (2022). Synthetic hydrogels engineered to promote collecting lymphatic vessel sprouting. Biomaterials *284*, 121483. https://doi.org/10.1016/j.biomaterials.2022.121483.

5. Jung, Y., Ji, H., Chen, Z., Fai Chan, H., Atchison, L., Klitzman, B., Truskey, G., and Leong, K.W. (2015). Scaffold-free, Human Mesenchymal Stem Cell-Based Tissue Engineered Blood Vessels. Sci. Rep. *5*, 15116. https://doi.org/10.1038/srep15116.

6. Gibot, L., Galbraith, T., Kloos, B., Das, S., Lacroix, D.A., Auger, F.A., and Skobe, M. (2016). Cell-based approach for 3D reconstruction of lymphatic capillaries *in vitro* reveals distinct functions of HGF and VEGF-C in lymphangiogenesis. Biomaterials *78*, 129–139. https://doi.org/10.1016/j.biomaterials.2015.11.027.

7. Marino, D., Luginbühl, J., Scola, S., Meuli, M., and Reichmann, E. (2014). Bioengineering Dermo-Epidermal Skin Grafts with Blood and Lymphatic Capillaries. Sci. Transl. Med. *6*, 221ra14. https://doi.org/10.1126/scitranslmed.3006894.

8. Matsusaki, M., Fujimoto, K., Shirakata, Y., Hirakawa, S., Hashimoto, K., and Akashi, M. (2015). Development of full-thickness human skin equivalents with blood and lymph-like capillary networks by cell coating technology. J. Biomed. Mater. Res. *103*, 3386–3396. https://doi.org/10.1002/jbm.a.35473.

9. Helm, C.-L.E., Zisch, A., and Swartz, M.A. (2007). Engineered blood and lymphatic capillaries in 3-D VEGF-fibrin-collagen matrices with interstitial flow. Biotechnol. Bioeng. *96*, 167–176. https://doi.org/10.1002/bit.21185.

10. Knezevic, L., Schaupper, M., Mühleder, S., Schimek, K., Hasenberg, T., Marx, U., Priglinger, E., Redl, H., and Holnthoner, W. (2017). Engineering Blood and Lymphatic Microvascular Networks in Fibrin Matrices. Front. Bioeng. Biotechnol. *5*, 25. https://doi.org/10.3389/fbioe.2017.00025.

11. Kim, I.G., Lee, J.Y., Lee, D.S., Kwon, J.Y., and Hwang, J.H. (2013). Extracorporeal Shock Wave Therapy Combined with Vascular Endothelial Growth Factor-C Hydrogel for Lymphangiogenesis. J. Vasc. Res. *50*, 124–133. https://doi.org/10.1159/000343699.

12. Hall, E., Mendiola, K., Lightsey, N.K., and Hanjaya-Putra, D. (2024). Mimicking blood and lymphatic vasculatures using microfluidic systems. Biomicrofluidics *18*, 031502. https://doi.org/10.1063/5.0175154.

13. Kraus, S., and Lee, E. (2023). A human initial lymphatic chip reveals distinct mechanisms of primary lymphatic valve dysfunction in acute and chronic inflammation. Lab Chip *23*, 5180–5194. https://doi.org/10.1039/D3LC00486D.

14. Sabine, A., Saygili Demir, C., and Petrova, T.V. (2016). Endothelial Cell Responses to Biomechanical Forces in Lymphatic Vessels. Antioxid. Redox Signal. *25*, 451–465. https://doi.org/10.1089/ars.2016.6685.

15. Angeli, V., and Lim, H.Y. (2023). Biomechanical control of lymphatic vessel physiology and functions. Cell. Mol. Immunol. *20*, 1051–1062. https://doi.org/10.1038/s41423-023-01042-9.

16. Moore, J.E., and Bertram, C.D. (2018). Lymphatic System Flows. Annu. Rev. Fluid Mech. *50*, 459–482. https://doi.org/10.1146/annurev-fluid-122316-045259.

17. Breslin, J.W. (2014). Mechanical Forces and Lymphatic Transport. Microvasc. Res *96*, 46–54. https://doi.org/10.1016/j.mvr.2014.07.013.

18. Scallan, J.P., Zawieja, S.D., Castorena-Gonzalez, J.A., and Davis, M.J. (2016). Lymphatic pumping: mechanics, mechanisms and malfunction. J. Physiol. *594*, 5749–5768. https://doi.org/10.1113/JP272088.

19. Bazigou, E., Wilson, J.T., and Moore, J.E. (2014). Primary and secondary lymphatic valve development: Molecular, functional and mechanical insights. Microvasc. Res. *96*, 38–45. https://doi.org/10.1016/j.mvr.2014.07.008.

20. Zawieja, D.C. (2009). Contractile Physiology of Lymphatics. Lymphatic Res. Biol. *7*, 87–96. https://doi.org/10.1089/lrb.2009.0007.

21. Lutter, S., Xie, S., Tatin, F., and Makinen, T. (2012). Smooth muscle–endothelial cell communication activates Reelin signaling and regulates lymphatic vessel formation. J. Cell Biol. *197*, 837–849. https://doi.org/10.1083/jcb.201110132.

22. Bazigou, E., Xie, S., Chen, C., Weston, A., Miura, N., Sorokin, L., Adams, R., Muro, A.F., Sheppard, D., and Makinen, T. (2009). Integrin-alpha9 is required for fibronectin matrix assembly during lymphatic valve morphogenesis. Dev. Cell *17*, 175–186. https://doi.org/10.1016/j.devcel.2009.06.017.

23. Alderfer, L., Russo, E., Archilla, A., Coe, B., and Hanjaya-Putra, D. (2021). Matrix stiffness primes lymphatic tube formation directed by vascular endothelial growth factor-C. FASEB J. *35*, e21498. https://doi.org/10.1096/fj.202002426RR.

24. Saha, S., Fan, F., Alderfer, L., Graham, F., Hall, E., and Hanjaya-Putra, D. (2023). Synthetic hyaluronic acid coating preserves the phenotypes of lymphatic endothelial cells. Biomater. Sci. *11*, 7346–7357. https://doi.org/10.1039/D3BM00873H.

25. Mäkinen, T., Veikkola, T., Mustjoki, S., Karpanen, T., Catimel, B., Nice, E.C., Wise, L., Mercer, A., Kowalski, H., Kerjaschki, D., et al. (2001). Isolated lymphatic endothelial cells transduce growth, survival and migratory signals via the VEGF-C/D receptor VEGFR-3. EMBO J. *20*, 4762–4773. https://doi.org/10.1093/emboj/20.17.4762.

26. Wu, M., Du, Y., Liu, Y., He, Y., Yang, C., Wang, W., and Gao, F. (2014). Low Molecular Weight Hyaluronan Induces Lymphangiogenesis through LYVE-1-Mediated Signaling Pathways. PLoS One *9*, e92857. https://doi.org/10.1371/journal.pone.0092857.

27. Lawrance, W., Banerji, S., Day, A.J., Bhattacharjee, S., and Jackson, D.G. (2016). Binding of Hyaluronan to the Native Lymphatic Vessel Endothelial Receptor LYVE-1 Is Critically Dependent on Receptor Clustering and Hyaluronan Organization. J. Biol. Chem. *291*, 8014–8030. https://doi.org/10.1074/jbc.M115.708305.

28. Pang, X., Li, W., Chang, L., Gautrot, J.E., Wang, W., and Azevedo, H.S. (2021). Hyaluronan (HA) Immobilized on Surfaces via Self-Assembled Monolayers of HA-Binding Peptide Modulates Endothelial Cell Spreading and Migration through Focal Adhesion. ACS Appl. Mater. Interfaces *13*, 25792–25804. https://doi.org/10.1021/acsami.1c05574.

29. Bayer, I.S. (2020). Hyaluronic Acid and Controlled Release: A Review. Molecules *25*, 2649. https://doi.org/10.3390/molecules25112649.

30. Gramlich, W.M., Kim, I.L., and Burdick, J.A. (2013). Synthesis and orthogonal photopatterning of hyaluronic acid hydrogels with thiol-norbornene chemistry. Biomaterials *34*, 9803–9811. https://doi.org/10.1016/j.biomaterials.2013.08.089.

31. Kwon, M.Y., Wang, C., Galarraga, J.H., Puré, E., Han, L., and Burdick, J.A. (2019). Influence of hyaluronic acid modification on CD44 binding towards the design of hydrogel biomaterials. Biomaterials *222*, 119451. https://doi.org/10.1016/j.biomaterials.2019.119451.

32. Chen, Y., Wang, Q., Ning, F., Du, C., Chen, M., Feng, C., and Dong, C.-M. (2024). Dynamic Hyaluronic Acid Hydrogels for Comprehensively Regulating Inflammation, Angiogenesis, and Metabolism to Effectively Proheal Diabetic Wounds. ACS Appl. Mater. Interfaces *16*, 70256–70273. https://doi.org/10.1021/acsami.4c15674.

33. Sabine, A., Agalarov, Y., Maby-El Hajjami, H., Jaquet, M., Hägerling, R., Pollmann, C., Bebber, D., Pfenniger, A., Miura, N., Dormond, O., et al. (2012). Mechanotransduction, PROX1, and FOXC2 Cooperate to Control Connexin37 and Calcineurin during Lymphatic-Valve Formation. Dev. Cell *22*, 430–445. https://doi.org/10.1016/j.devcel.2011.12.020.

34. Sweet, D.T., Jiménez, J.M., Chang, J., Hess, P.R., Mericko-Ishizuka, P., Fu, J., Xia, L., Davies, P.F., and Kahn, M.L. (2015). Lymph flow regulates collecting lymphatic vessel maturation in vivo. J. Clin. Investig. *125*, 2995–3007. https://doi.org/10.1172/JCI79386.

35. Sabine, A., Bovay, E., Demir, C.S., Kimura, W., Jaquet, M., Agalarov, Y., Zangger, N., Scallan, J.P., Graber, W., Gulpinar, E., et al. (2015). FOXC2 and fluid shear stress stabilize postnatal lymphatic vasculature. J. Clin. Investig. *125*, 3861–3877. https://doi.org/10.1172/JCI80454.

36. Kazenwadel, J., Betterman, K.L., Chong, C.-E., Stokes, P.H., Lee, Y.K., Secker, G.A., Agalarov, Y., Demir, C.S., Lawrence, D.M., Sutton, D.L., et al. (2015). GATA2 is required for lymphatic vessel valve development and maintenance. J. Clin. Investig. *125*, 2979–2994. https://doi.org/10.1172/JCI78888.

37. Saygili Demir, C., Sabine, A., Gong, M., Dormond, O., and Petrova, T.V. (2023). Mechanosensitive mTORC1 signaling maintains lymphatic valves. J. Cell Biol. *222*, e202207049. https://doi.org/10.1083/jcb.202207049.

38. Nonomura, K., Lukacs, V., Sweet, D.T., Goddard, L.M., Kanie, A., Whitwam, T., Ranade, S.S., Fujimori, T., Kahn, M.L., and Patapoutian, A. (2018). Mechanically activated ion channel PIEZO1 is required for lymphatic valve formation. Proc. Natl. Acad. Sci. USA *115*, 12817–12822. https://doi.org/10.1073/pnas.1817070115.

39. Murtomaki, A., Uh, M.K., Kitajewski, C., Zhao, J., Nagasaki, T., Shawber, C.J., and Kitajewski, J. (2014). Notch signaling functions in lymphatic valve formation. Development *141*, 2446–2451. https://doi.org/10.1242/dev.101188.

40. Norrmén, C., Ivanov, K.I., Cheng, J., Zangger, N., Delorenzi, M., Jaquet, M., Miura, N., Puolakkainen, P., Horsley, V., Hu, J., et al. (2009). FOXC2 controls formation and maturation of lymphatic collecting vessels through cooperation with NFATc1. J. Cell Biol. *185*, 439–457. https://doi.org/10.1083/jcb.200901104.

41. Choi, D., Park, E., Yu, R.P., Cooper, M.N., Cho, I.-T., Choi, J., Yu, J., Zhao, L., Yum, J.-E.I., Yu, J.S., et al. (2022). Piezo1-Regulated Mechanotransduction Controls Flow-Activated Lymphatic Expansion. Circ. Res. *131*, e2–e21. https://doi.org/10.1161/CIRCRESAHA.121.320565.

42. Pujari, A., Smith, A.F., Hall, J.D., Mei, P., Chau, K., Nguyen, D.T., Sweet, D.T., and Jiménez, J.M. (2020). Lymphatic Valves Separate Lymph Flow Into a Central Stream and a Slow-Moving Peri-Valvular Milieu. J. Biomech. Eng. *142*, 100805. https://doi.org/10.1115/1.4048028.

43. Yang, Y., Cha, B., Motawe, Z.Y., Srinivasan, R.S., and Scallan, J.P. (2019). VE-Cadherin Is Required for Lymphatic Valve Formation and Maintenance. Cell Rep. *28*, 2397–2412.e4. https://doi.org/10.1016/j.celrep.2019.07.072.

44. Baluk, P., Fuxe, J., Hashizume, H., Romano, T., Lashnits, E., Butz, S., Vestweber, D., Corada, M., Molendini, C., Dejana, E., and McDonald, D.M. (2007). Functionally specialized junctions between endothelial cells of lymphatic vessels. J. Exp. Med. *204*, 2349–2362. https://doi.org/10.1084/jem.20062596.

45. Norden, P.R., Sabine, A., Wang, Y., Demir, C.S., Liu, T., Petrova, T.V., and Kume, T. (2020). Shear stimulation of FOXC1 and FOXC2 differentially regulates cytoskeletal activity during lymphatic valve maturation. eLife *9*, e53814. https://doi.org/10.7554/eLife.53814.

46. Baluk, P., Yao, L.-C., Flores, J.C., Choi, D., Hong, Y.-K., and McDonald, D.M. (2017). Rapamycin reversal of VEGF-C–driven lymphatic anomalies in the respiratory tract. JCI Insight *2*, e90103. https://doi.org/10.1172/jci.insight.90103.

47. Michalaki, E., Surya, V.N., Fuller, G.G., and Dunn, A.R. (2020). Perpendicular alignment of lymphatic endothelial cells in response to spatial gradients in wall shear stress. Commun. Biol. *3*, 57–59. https://doi.org/10.1038/s42003-019-0732-8.

48. Dixon, J.B., Greiner, S.T., Gashev, A.A., Cote, G.L., Moore, J.E., and Zawieja, D.C. (2006). Lymph flow, shear stress, and lymphocyte velocity in rat mesenteric prenodal lymphatics. Microcirculation *13*, 597–610. https://doi.org/10.1080/10739680600893909.

49. Selahi, A., Chakraborty, S., Muthuchamy, M., Zawieja, D.C., and Jain, A. (2022). Intracellular calcium dynamics of lymphatic endothelial and muscle cells co-cultured in a Lymphangion-Chip under pulsatile flow. Analyst *147*, 2953–2965. https://doi.org/10.1039/D2AN00396A.

50. Blatter, C., Meijer, E.F.J., Nam, A.S., Jones, D., Bouma, B.E., Padera, T.P., and Vakoc, B.J. (2016). In vivo label-free measurement of lymph flow velocity and volumetric flow rates using Doppler optical coherence tomography. Sci. Rep. *6*, 29035. https://doi.org/10.1038/srep29035.

51. Cappello, V., Marchetti, L., Parlanti, P., Landi, S., Tonazzini, I., Cecchini, M., Piazza, V., and Gemmi, M. (2016). Ultrastructural Characterization of the Lower Motor System in a Mouse Model of Krabbe Disease. Sci. Rep. *6*, 1. https://doi.org/10.1038/s41598-016-0001-8.

52. Dixon, J.B., Zawieja, D.C., Gashev, A.A., and Coté, G.L. (2005). Measuring microlymphatic flow using fast video microscopy. J. Biomed. Opt. *10*, 064016. https://doi.org/10.1117/1.2135791.

53. Dixon, J.B., Gashev, A.A., Zawieja, D.C., Moore, J.E., and Coté, G.L. (2007). Image correlation algorithm for measuring lymphocyte velocity and diameter changes in contracting microlymphatics. Ann. Biomed. Eng. *35*, 387–396. https://doi.org/10.1007/s10439-006-9225-2.

54. Zhang, J., Patel, J.M., and Block, E.R. (2002). Enhanced apoptosis in prolonged cultures of senescent porcine pulmonary artery endothelial cells. Mech. Ageing Dev. *123*, 613–625. https://doi.org/10.1016/S0047-6374(01)00412-2.

55. Frye, M., Taddei, A., Dierkes, C., Martinez-Corral, I., Fielden, M., Ortsäter, H., Kazenwadel, J., Calado, D.P., Ostergaard, P., Salminen, M., et al. (2018). Matrix stiffness controls lymphatic vessel formation through regulation of a GATA2-dependent transcriptional program. Nat. Commun. *9*, 1511. https://doi.org/10.1038/s41467-018-03959-6.

56. Selahi, A., and Jain, A. (2023). Engineered models of the lymphatic vascular system: Past, present, and future. Microcirculation *30*, e12793. https://doi.org/10.1111/micc.12793.

57. Norden, P.R., and Kume, T. (2020). Molecular Mechanisms Controlling Lymphatic Endothelial Junction Integrity. Front. Cell Dev. Biol. *8*, 627647. https://doi.org/10.3389/fcell.2020.627647.

58. Frye, M., Stritt, S., Ortsäter, H., Hernandez Vasquez, M., Kaakinen, M., Vicente, A., Wiseman, J., Eklund, L., Martínez-Torrecuadrada, J.L., Vestweber, D., and Mäkinen, T. (2020). EphrinB2-EphB4 signalling provides Rho-mediated homeostatic control of lymphatic endothelial cell junction integrity. eLife *9*, e57732. https://doi.org/10.7554/eLife.57732.

59. Petrova, T.V., Mäkinen, T., Mäkelä, T.P., Saarela, J., Virtanen, I., Ferrell, R.E., Finegold, D.N., Kerjaschki, D., Ylä-Herttuala, S., and Alitalo, K. (2002). Lymphatic endothelial reprogramming of vascular endothelial cells by the Prox-1 homeobox transcription factor. EMBO J. *21*, 4593–4599. https://doi.org/10.1093/emboj/cdf470.

60. Shao, Y., Mann, J.M., Chen, W., and Fu, J. (2014). Global architecture of the F-actin cytoskeleton regulates cell shape-dependent endothelial mechanotransduction. Integr. Biol. *6*, 300–311. https://doi.org/10.1039/c3ib40223a.

61. Harris, A.R., Jreij, P., and Fletcher, D.A. (2018). Mechanotransduction by the Actin Cytoskeleton: Converting Mechanical Stimuli into Biochemical Signals. Annu. Rev. Biophys. *47*, 617–631. https://doi.org/10.1146/annurev-biophys-070816-033547.

62. Schoofs, H., Daubel, N., Schnabellehner, S., Grönloh, M.L.B., Palacios Martínez, S., Halme, A., Marks, A.M., Jeansson, M., Barcos, S., Brakebusch, C., et al. (2025). Dynamic cytoskeletal regulation of cell shape supports resilience of lymphatic endothelium. Nature *641*, 465–475. https://doi.org/10.1038/s41586-025-08724-6.

63. Wick, N., Haluza, D., Gurnhofer, E., Raab, I., Kasimir, M.-T., Prinz, M., Steiner, C.-W., Reinisch, C., Howorka, A., Giovanoli, P., et al. (2008). Lymphatic Precollectors Contain a Novel, Specialized Subpopulation of Podoplaninlow, CCL27-Expressing Lymphatic Endothelial Cells. Am. J. Pathol. *173*, 1202–1209. https://doi.org/10.2353/ajpath.2008.080101.

64. Petrova, T.V., and Koh, G.Y. (2020). Biological functions of lymphatic vessels. Science *369*, eaax4063. https://doi.org/10.1126/science.aax4063.

65. Han, F., Simeroth, S., Zhu, J., Gryniuk, I., Pranay, A., Chen, W., Wang, Y., Cai, Y., Shen, Z., Wang, G., et al. (2025). Lymphatic endothelial mTORC1 instructs metabolic and developmental signaling during lymphangiogenesis. Dev. Cell *60*, 2331–2347.e6, *0*. https://doi.org/10.1016/j.devcel.2025.04.012.

66. Smith, S.F., Islam, A.F.M.T., Alimukhamedov, S., Weiss, E.T., and Charest, P.G. (2024). Molecular determinants of Ras-mTORC2 signaling. J. Biol. Chem. *300*, 107423. https://doi.org/10.1016/j.jbc.2024.107423.

67. Calvisi, D.F., Wang, C., Ho, C., Ladu, S., Lee, S.A., Mattu, S., Destefanis, G., Delogu, S., Zimmermann, A., Ericsson, J., et al. (2011). Increased Lipogenesis, Induced by AKT-mTORC1-RPS6 Signaling, Promotes Development of Human Hepatocellular Carcinoma. Gastroenterology *140*, 1071–1083. https://doi.org/10.1053/j.gastro.2010.12.006.

68. Sun, S., Chen, S., Liu, F., Wu, H., McHugh, J., Bergin, I.L., Gupta, A., Adams, D., and Guan, J.-L. (2015). Constitutive Activation of mTORC1 in Endothelial Cells Leads to the Development and Progression of Lymphangiosarcoma through VEGF Autocrine Signaling. Cancer Cell *28*, 758–772. https://doi.org/10.1016/j.ccell.2015.10.004.

69. Scallan, J.P., Knauer, L.A., Hou, H., Castorena-Gonzalez, J.A., Davis, M.J., and Yang, Y. (2021). *Foxo1* deletion promotes the growth of new lymphatic valves. J. Clin. Investig. *131*, e142341. https://doi.org/10.1172/JCI142341.

70. Hernández Vásquez, M.N., Ulvmar, M.H., González-Loyola, A., Kritikos, I., Sun, Y., He, L., Halin, C., Petrova, T.V., and Mäkinen, T. (2021). Transcription factor FOXP2 is a flow-induced regulator of collecting lymphatic vessels. EMBO J. *40*, EMBJ2020107192. https://doi.org/10.15252/embj.2020107192.

71. Fathi, P., Holland, G., Pan, D., and Esch, M.B. (2020). Lymphatic Vessel on a Chip with Capability for Exposure to Cyclic Fluidic Flow. ACS Appl. Bio Mater. *3*, 6697–6707. https://doi.org/10.1021/acsabm.0c00609.

72. Henderson, A.R., Choi, H., and Lee, E. (2020). Blood and Lymphatic Vasculatures On-Chip Platforms and Their Applications for Organ-Specific In Vitro Modeling. Micromachines *11*, 147. https://doi.org/10.3390/mi11020147.

73. Tronolone, J.J., Mohamed, N., and Jain, A. (2024). Engineering Lymphangiogenesis-On-Chip: The Independent and Cooperative Regulation by Biochemical Factors, Gradients, and Interstitial Fluid Flow. Adv. Biol. *8*, 2400031. https://doi.org/10.1002/adbi.202400031.

74. Breslin, J.W., and Kurtz, K.M. (2009). Lymphatic Endothelial Cells Adapt Their Barrier Function in Response to Changes in Shear Stress. Lymphatic Res. Biol. *7*, 229–237. https://doi.org/10.1089/lrb.2009.0015.

75. Miteva, D.O., Rutkowski, J.M., Dixon, J.B., Kilarski, W., Shields, J.D., and Swartz, M.A. (2010). Transmural Flow Modulates Cell and Fluid Transport Functions of Lymphatic Endothelium. Circ. Res. *106*, 920–931. https://doi.org/10.1161/CIRCRESAHA.109.207274.

76. Stanly, T.A., Fritzsche, M., Banerji, S., Shrestha, D., Schneider, F., Eggeling, C., and Jackson, D.G. (2020). The cortical actin network regulates avidity-dependent binding of hyaluronan by the lymphatic vessel endothelial receptor LYVE-1. J. Biol. Chem. *295*, 5036–5050. https://doi.org/10.1074/jbc.RA119.011992.

77. Tammela, T., and Alitalo, K. (2010). Lymphangiogenesis: Molecular Mechanisms and Future Promise. Cell *140*, 460–476. https://doi.org/10.1016/j.cell.2010.01.045.

78. Tacconi, C., He, Y., Ducoli, L., and Detmar, M. (2021). Epigenetic regulation of the lineage specificity of primary human dermal lymphatic and blood vascular endothelial cells. Angiogenesis *24*, 67–82. https://doi.org/10.1007/s10456-020-09743-9.

79. Baxter, S.A., Cheung, D.Y., Bocangel, P., Kim, H.K., Herbert, K., Douville, J.M., Jangamreddy, J.R., Zhang, S., Eisenstat, D.D., and Wigle, J.T. (2011). Regulation of the lymphatic endothelial cell cycle by the PROX1 homeodomain protein. Biochim. Biophys. Acta *1813*, 201–212. https://doi.org/10.1016/j.bbamcr.2010.10.015.

80. Ducoli, L., and Detmar, M. (2021). Beyond PROX1: transcriptional, epigenetic, and noncoding RNA regulation of lymphatic identity and function. Dev. Cell *56*, 406–426. https://doi.org/10.1016/j.devcel.2021.01.018.

81. Cha, B., Geng, X., Mahamud, M.R., Fu, J., Mukherjee, A., Kim, Y., Jho, E.H., Kim, T.H., Kahn, M.L., Xia, L., et al. (2016). Mechanotransduction activates canonical Wnt/β-catenin signaling to promote lymphatic vascular patterning and the development of lymphatic and lymphovenous valves. Genes Dev. *30*, 1454–1469. https://doi.org/10.1101/gad.282400.116.

82. Wang, C., Baker, B.M., Chen, C.S., and Schwartz, M.A. (2013). Endothelial cell sensing of flow direction. Arterioscler. Thromb. Vasc. Biol. *33*, 2130–2136. https://doi.org/10.1161/ATVBAHA.113.301826.

83. Baeyens, N., Bandyopadhyay, C., Coon, B.G., Yun, S., and Schwartz, M.A. (2016). Endothelial fluid shear stress sensing in vascular health and disease. J. Clin. Investig. *126*, 821–828. https://doi.org/10.1172/JCI83083.

84. Ivanov, K.I., Agalarov, Y., Valmu, L., Samuilova, O., Liebl, J., Houhou, N., Maby-El Hajjami, H., Norrmén, C., Jaquet, M., Miura, N., et al. (2013). Phosphorylation Regulates FOXC2-Mediated Transcription in Lymphatic Endothelial Cells. Mol. Cell Biol. *33*, 3749–3761. https://doi.org/10.1128/MCB.01387-12.

85. Bernier-Latmani, J., Cisarovsky, C., Demir, C.S., Bruand, M., Jaquet, M., Davanture, S., Ragusa, S., Siegert, S., Dormond, O., Benedito, R., et al. (2015). DLL4 promotes continuous adult intestinal lacteal regeneration and dietary fat transport. J. Clin. Investig. *125*, 4572–4586. https://doi.org/10.1172/JCI82045.

86. Sweet, D.T., Hall, J.D., Welsh, J., Kahn, M.L., and Jiménez, J.M. (2018). Investigating Effects of Fluid Shear Stress on Lymphatic Endothelial Cells. Methods Mol. Biol. *1846*, 213–227. https://doi.org/10.1007/978-1-4939-8712-2_14.

87. Montes, D., Saha, S., Taglione, A., Jeong, D.P., Chen, L., Fan, F., Chang, H.-C., and Hanjaya-Putra, D. (2025). Tuning the Morphological Properties of Granular Hydrogels to Control Lymphatic Capillary Formation. Adv. Mater. Interfac. *12*, 2401037. https://doi.org/10.1002/admi.202401037.

88. Deng, Y., Zhou, Y., Tay, H.M., Wang, H., Chen, J., Luo, Y., Zhang, H., Zhang, C., Ibayashi, Y., Paiè, P., et al. (2026). Real-time imaging of platelet dynamics in engineered arterial, venous, and cancer-associated thrombotic microenvironments. Biofabrication *18*, 015022. https://doi.org/10.1088/1758-5090/ae302c.

89. Pandian, N.K.R., Walther, B.K., Suresh, R., Cooke, J.P., and Jain, A. (2020). Microengineered Human Vein-Chip Recreates Venous Valve Architecture and Its Contribution to Thrombosis. Small *16*, e2003401. https://doi.org/10.1002/smll.202003401.

90. Niec, R.E., Chu, T., Schernthanner, M., Gur-Cohen, S., Hidalgo, L., Pasolli, H.A., Luckett, K.A., Wang, Z., Bhalla, S.R., Cambuli, F., et al. (2022). Lymphatics act as a signaling hub to regulate intestinal stem cell activity. Cell Stem Cell *29*, 1067–1082.e18. https://doi.org/10.1016/j.stem.2022.05.007.

91. Ulvmar, M.H., and Mäkinen, T. (2016). Heterogeneity in the lymphatic vascular system and its origin. Cardiovasc. Res. *111*, 310–321. https://doi.org/10.1093/cvr/cvw175.

92. Podder, P.S., Bhadra, D., Pal, S., Klimberg, V.S., and Stolarz, A.J. (2025). Clinical Relevance of Animal Models of Lymphatic Dysfunction and Lymphedema. Microcirculation *32*, e70009. https://doi.org/10.1111/micc.70009.

93. Alderfer, L., Saha, S., Fan, F., Wu, J., Littlepage, L.E., and Hanjaya-Putra, D. (2024). Multi-parameter tunable synthetic matrix for engineering lymphatic vessels. Commun. Biol. *7*, 1262. https://doi.org/10.1038/s42003-024-06935-7.

94. Weiler, M.J., Cribb, M.T., Nepiyushchikh, Z., Nelson, T.S., and Dixon, J.B. (2019). A novel mouse tail lymphedema model for observing lymphatic pump failure during lymphedema development. Sci. Rep. *9*, 10405. https://doi.org/10.1038/s41598-019-46797-2.

95. Dougherty, R., and Kunzelmann, K.-H. (2007). Computing Local Thickness of 3D Structures with ImageJ. Micro *13*, 1678–1679. https://doi.org/10.1017/S1431927607074430.

96. Arganda-Carreras, I., Fernández-González, R., Muñoz-Barrutia, A., and Ortiz-De-Solorzano, C. (2010). 3D reconstruction of histological sections: Application to mammary gland tissue. Microsc. Res. Tech. *73*, 1019–1029. https://doi.org/10.1002/jemt.20829.

97. Rezakhaniha, R., Agianniotis, A., Schrauwen, J.T.C., Griffa, A., Sage, D., Bouten, C.V.C., van de Vosse, F.N., Unser, M., and Stergiopulos, N. (2012). Experimental investigation of collagen waviness and orientation in the arterial adventitia using confocal laser scanning microscopy. Biomech. Model. Mechanobiol. *11*, 461–473. https://doi.org/10.1007/s10237-011-0325-z.

Please cite this article in press as: Lightsey et al., Engineering lymphatic collecting vessel phenotypes through combined hyaluronic acid cues and oscillatory shear stress, Cell Reports Methods (2026), https://doi.org/10.1016/j.crmeth.2026.101574

STAR★METHODS

KEY RESOURCES TABLE

REAGENT or RESOURCE	SOURCE	IDENTIFIER
Antibodies		
Goat anti-human PROX1	R&D Systems	AF2727; RRID: AB_2170716
Rabbit anti-human VE-Cadherin	Abcam	ab232880
Mouse anti-human FOXC2	R&D Systems	MAB5044; RRID: AB_10888663
Rabbit anti-human LYVE-1	Abcam	ab219556; RRID: AB_2884014
Mouse anti-human PDPN	Abcam	ab10288; RRID: AB_297027
Phalloidin-iFluor 488 Reagent	Abcam	ab176753
Rabbit anti-human Ki67	Abcam	ab15580; RRID: AB_443209
Rabbit anti-human Phospho-S6 Ribosomal Protein (Ser240/244)	Cell Signaling	5364; RRID: AB_10694233
Mouse anti-human Ki67	Cell Signaling	9449; RRID: AB_2797703
Chemicals, peptides, and recombinant proteins		
Dopamine-modified hyaluronic acid	Saha et al.[24]/Hanjaya-Putra Lab	N/A
Fibronectin, Human	Corning	356008
Rapamycin, 98+%	Thermo Scientific Chemicals	J62473.MF
Critical commercial assays		
TaqMan™ Array Human Angiogenesis Panel	Applied Biosystems™	4378710
Experimental models: Cell lines		
Human Dermal Lymphatic Endothelial Cells (HDLEC)	PromoCell	C-12216
Oligonucleotides		
GAPDH	Thermo Fisher Scientific	Hs99999905_m1
HPRT1	Thermo Fisher Scientific	Hs99999909_m1
GUSB	Thermo Fisher Scientific	Hs99999908_m1
FGA	Thermo Fisher Scientific	Hs00241027_m1
PLG	Thermo Fisher Scientific	Hs00264877_m1
SERPINC1	Thermo Fisher Scientific	Hs00166654_m1
PRL	Thermo Fisher Scientific	Hs00168730_m1
MMP2	Thermo Fisher Scientific	Hs00234422_m1
ANG	Thermo Fisher Scientific	Hs02379000_s1
ANGPT1	Thermo Fisher Scientific	Hs00181613_m1
Additional primers within TaqMan™ Array Human Angiogenesis Panel	Thermo Fisher Scientific	see Table S1
Software and algorithms		
ImageJ	Schindelin et al.[95]	https://imagej.net/downloads
MATLAB R2023	MathWorks	https://www.mathworks.com/products/matlab.html
Local Thickness ImageJ plugin	Dougherty and Kunzelmann[95]	https://imagej.net/downloads
Analyze Skeleton ImageJ plugin	Arganda-Carreras et al.[96]	https://imagej.net/downloads
OrientationJ	Rezakhaniha et al.[97]	https://bigwww.epfl.ch/demo/orientation/
GraphPad Prism Version 11	GraphPad by Dotmatics	https://www.graphpad.com/
Thermo Fisher Connect Platform	Thermo Fisher Scientific	https://www.thermofisher.com/us/en/home/digital-science/thermo-fisher-connect.html

(*Continued on next page*)

Please cite this article in press as: Lightsey et al., Engineering lymphatic collecting vessel phenotypes through combined hyaluronic acid cues and oscillatory shear stress, Cell Reports Methods (2026), https://doi.org/10.1016/j.crmeth.2026.101574

Continued

REAGENT or RESOURCE	SOURCE	IDENTIFIER
Other		
ibidi Pump System	ibidi	10902
μ-Slide I Luer 0.6	ibidi	80186
Red Perfusion Set	ibidi	10962
Gray Perfusion Set	ibidi	10968

EXPERIMENTAL MODEL AND STUDY PARTICIPANT DETAILS

Cell source and culture

Human male donor dermal LECs from juvenile foreskin (PromoCell, Heidelberg, Germany) were expanded and used for experiments between passages 6 and 9. Primary cells were authenticated by PromoCell. Male-specific donor cells are primarily used due to the limited sources of juvenile dermal LECs from female patients. Juvenile dermal LECs were used for optimal *in vitro* culturing. Sex-neutral sources of juvenile cells are not readily available, but we infer there would be limited changes in results regardless of the source.

Human LECs were grown in endothelial cell growth medium MV2 (C-22022, EGM MV2; PromoCell) containing MycoZap Plus-CL (VZA-2011; Lonza, Cologne Germany) and incubated at 37°C with 5% CO2. Cell line was routinely tested for mycoplasma contamination and were negative throughout this study.

Cell culture under flow set up

Human LECs were seeded on fibronectin-coated (40 μg/mL) or HA-DP coated (5 mg/mL) microfluidic channels (ibidi μ-Slide I 0.6 Luer) at 500K–800K/mL before onset of experiment to reach confluency. Three slides per condition were subjected to oscillatory flow either at 0.5 dyn/cm^2 (gray perfusion set, ibidi) or 10 dyn/cm^2 (red perfusion set, ibidi) at 2 Hz with EGM MV2 media in a parallel plate flow-chamber system (ibidi Pump System) or maintained at static conditions for 48 h in an incubator at 37°C with 5% CO2. After 48 h, slides were collected for various analyses. For the treatment of rapamycin, EGM MV2 media had a final concentration of 10 nM rapamycin and was given to cells on the onset of experiment then treated for 48 h at the previously described conditions.

METHOD DETAILS

Dopamine-modified hyaluronic acid synthesis

Conjugation of dopamine was completed as precisely described in Saha et al.[24] Briefly, HA was dissolved in MES buffer and ethanol was added then brought at equilibrium in room temperature. DMTMM was added to activate HA then dopamine was added after an incubation of 30 min then mixture was stirred at room temperature overnight. HA-DP was purified by dialysis, lyophilized, and stored in −20°C. H-NMR analysis confirmed its degree of substitution and presence of dopamine (Figure S1).

Extracellular matrix coating

Fibronectin was dissolved in PBS at 40 μg/mL (80 μg/mL for supplemental information) and polymerized via room temperature incubation for 30+ minutes. HA-DP was dissolved in H2O (5 mg/mL) and polymerized via the addition of 7M NaOH (1.2 μL per slide) followed by an overnight incubation at 37°C. Slides were rinsed with their respective solvents 3–5 times.

Immunofluorescent imaging

To analyze LEC phenotype, slides from the previously mentioned flow experiments were fixed with 3.7% formaldehyde, blocked with 1% BSA, permeabilized with 0.1% Triton X-, and stained for PROX1 (1:200), FOXC2 (1:100), VE-CAD (1:100), PDPN (1:500), and LYVE-1 (1:1000). To analyze F-actin directionality and intensity, phalloidin (1:1000) was used. To analyze Ki67 activity, anti-Ki67 antibodies were used (mouse antibody diluted at 1:1600 and rabbit antibody diluted at 1:200). To analyze mTORC1 activity, Phospho-S6 Ribosomal Protein (pS6) antibody (1:800) was used. Antibody details in key resources table. Slides were rinsed in 1× PBS and counterstained with DAPI (Thermo Fisher, 300 nM). Slides were imaged at 10× and 20× magnification with the ECHO Revolve microscope and at 10× magnification with the Nikon AX-R Confocal microscope.

Gene expression

Slides from the previously mentioned flow experiments were lysed and each experimental condition, containing 3 slides each, were pooled together for RNA isolation. Samples were analyzed with real-time qRT-PCR with replicate readings as previously described.[23] The TaqMan Array Human Angiogenesis Panel (Thermo Fisher) along with the TaqMan Universal PCR Master Mix (Thermo Fisher) was utilized to run 94 gene expression assays (assay and individual genes in Table S1 and key resources table) for genes associated

with angiogenesis and lymphangiogenesis. The relative expression was globally normalized within the array panel due to the large number of genes being profiled and analyzed using the ΔΔCt method in ThermoFisher Connect software. The control was set to the static FN-LEC group.

QUANTIFICATION AND STATISTICAL ANALYSIS

Image analysis

All image analyses were conducted on Fiji ImageJ2. Images were thresholded depending on analysis and background was subtracted for all images. Morphological assessments were conducted with the particle analysis tool, which included circularity and roundness values, on thresholded VE-CAD images. Cellular membrane thickness was assessed on thresholded VE-CAD images with Local Thickness ImageJ plugin.[95] Skeletonized structures of thresholded VE-CAD images was assessed with the Analyze Skeleton ImageJ plugin.[96] F-actin distribution was determined with the OrientationJ plugin[97] (Biomedical Image Group, EPFL, Switzerland). Integrated density values of fluorescence were calculated with the measurement tool and nuclear region of interests were found with the use of DAPI channel images. For perinuclear locations, a 1.5× scaling of nuclear region of interests were made and nuclear intensities were subtracted. For cytoplasmic locations, whole image areas were measured then subtracted by both nuclear and perinuclear intensities. For total intensity images, whole image areas were measured. Normalization of values were done with respect to the number of cells present in image for integrated density per cell determination and all images for each analysis had same total area sizes. To determine number of positive Ki67 cells, integrated density at the nuclear region of interests were filtered and counted. To determine nuclear/cytoplasm, perinuclear/cytoplasm, and nuclear/perinuclear ratios, normalized intensity values of nucleus or perinucleus was divided by normalized cytoplasm or perinuclear values per image.

Statistical analysis

Statistical analysis was performed with GraphPad Prism. For each coating and shear stress condition, three independent slides ($n = 3$) were used with 3–4 technical replicates per slide. Detailed statistical details and replicate definitions can be found in figure legends. Statistical comparisons were made using two-way analysis of variance (ANOVA) and followed with Tukey's multiple comparison test. Significance levels were set at the following: $^{*}p < 0.05$, $^{**}p < 0.01$, $^{***}p < 0.001$, $^{****}p < 0.0001$.

Statistical analysis for the volcano plot in Figure 5 was conducted on Thermo Fisher Connect software using a Student's *t* test between group of interest and static FN-LEC group. Significance levels were set at the following: $^{*}p < 0.05$.

ADDITIONAL RESOURCES

Figure Assembly BioRender was used to assemble all figures while any diagrams/depictions were made from BioRender and identified in the figure legend. All microscopic images were only assessed and prepared for print in ImageJ. All graphs were made in GraphPad or MATLAB.